Paper accepted for publication at Global Change Biology
https://doi.org/10.1111/gcb.16933

Asymmetric response of Amazon forest water and energy fluxes to wet and dry hydrological extremes reveals onset of a local drought-induced tipping point

Running Head: Tropical forest response to extreme events

Natalia Restrepo-Coupe[1,2], Bradley O'Donnell Christoffersen[4,5], Marcos Longo[7], Luciana F. Alves[6], Kleber Silva Campos[3], Alessandro C. da Araujo[8,9], Raimundo C. de Oliveira Jr.[8], Neill Prohaska[1,2], Rodrigo da Silva[3], Raphael Tapajos[3], Kenia T. Wiedemann[10], Steven C. Wofsy[10], Scott R. Saleska[1]

1. Department of Ecology and Evolutionary Biology, The University of Arizona, Tucson, AZ, USA
2. School of Life Sciences, University of Technology Sydney, Sydney, NSW, Australia
3. Department of Environmental Physics, University of Western Pará-UFOPA, Santarém, Pará, Brazil
4. Department of Biology, University of Texas Rio Grande Valley, Edinburg, TX, USA
5. Earth and Environmental Sciences Division, Los Alamos National Laboratory, Los Alamos, NM, USA
6. Institute of the Environment and Sustainability, University of California Los Angeles, Los Angeles, CA, USA
7. Climate and Ecosystem Sciences Division, Lawrence Berkeley National Laboratory, Berkeley, CA, USA
8. Brazilian Agricultural Research Corporation (Embrapa) Amazônia Oriental, Belém, Pará, Brazil
9. Instituto Nacional de Pesquisas da Amazônia (INPA), Manaus, Amazonas, Brazil
10. Department of Earth and Planetary Sciences, Harvard University, Massachusetts, MA, USA

Correspondence: Natalia Restrepo-Coupe
email: nataliacoupe@gmail.com, phone: +1 647 328 1494

Key words: Eddy covariance, water and energy flux seasonality, Amazonia, tropical forests, ecosystem-climate interactions, ENSO.

Type of Paper: Primary Research Article.

Abstract

Understanding the effects of intensification of Amazon basin hydrological cycling--manifest as increasingly frequent floods and droughts--on water and energy cycles of tropical forests is essential to meeting the challenge of predicting ecosystem responses to climate change, including forest "tipping points". Here, we investigated the impacts of hydrological extremes on forest function using 12+ years of observations (between 2001-2020) of water and energy fluxes from eddy covariance, along with associated ecological dynamics from biometry, at the Tapajós National Forest. Measurements encompass the strong 2015-2016 El Niño drought and La Niña 2008-2009 wet events. We found that the forest responded strongly to ENSO: Drought reduced water availability for evapotranspiration (*ET*) leading to large increases in sensible heat fluxes (*H*). Partitioning *ET* by an approach that assumes transpiration (*T*) is proportional to photosynthesis, we found that water stress-induced reductions in canopy conductance (*Gs*) drove *T* declines partly compensated by higher evaporation (*E*). By contrast, the abnormally wet La Niña period gave higher *T* and lower *E*, with little change in seasonal *ET*. Both ENSO events resulted in changes in forest structure, manifested as lower wet-season leaf area index. However, only during El Niño 2015-2016, we observed a breakdown in the strong meteorological control of transpiration fluxes (via energy availability and atmospheric demand) because of slowing vegetation functions (via shutdown of *Gs* and significant leaf shedding). Drought-reduced *T* and *Gs,* higher *H* and *E*, amplified by feedbacks with higher temperatures and vapor pressure deficits, signaled that forest function had crossed a threshold, from which it recovered slowly, with delay, post-drought. Identifying such tipping point onsets (beyond which future irreversible processes may occur) at local scale is crucial for predicting basin-scale threshold-crossing changes in forest energy and water cycling, leading to slow-down in forest function, potentially resulting in Amazon forests shifting into alternate degraded states.

1. Introduction

Recent studies report climate-change associated intensification of hydrological cycling in the Amazon basin -- with increasing frequency of both drought and floods (Barichivich et al., 2018; Gloor et al., 2013). Observations have revealed that Amazon vegetation communities are vulnerable to prolonged or repeated drought, leading to increased mortality (Esquivel-Muelbert et al., 2019; Phillips et al., 2009), decreasing forest function (Botía et al., 2022; Gatti et al., 2021) and changes in vegetation structure and/or species composition (Amigo, 2020; Brando et al., 2020; Esquivel-Muelbert et al., 2019; Yang et al., 2022). Models also indicate that these droughts may trigger basin-wide ecosystem degradation (Staal et al., 2023), which can lead to a "tipping point" -- an abrupt transition in ecosystem function to an alternate stable but degraded state that is difficult to reverse (Cooper et al., 2020; Hirota et al., 2021; Lovejoy and Nobre, 2018; Oyama and Nobre, 2003). Here, we ask whether water limitation of tree communities during drought -- often associated with reductions in transpiration with significant feedback effects -- could be a tipping point mechanism. This question is motivated by consideration of the many ecosystem-atmosphere interactions, that may include: (1) further reductions in precipitation due to the loss of transpiration-driven recycling of rainwater back to the atmosphere (an estimated one-quarter to one-third of the basin-wide rainfall is recycled from upwind evapotranspiration (Cox et al., 2008; Eltahir and Bras, 1994; Makarieva et al., 2023; Smith et al., 2023; Trenberth, 1999; van der Ent et al., 2010); (2) reductions in land-derived moisture that cause forests to become net carbon sources, contributing to their degradation (Gatti et al., 2021; Staal et al., 2023) and (3) changes in the partition of available energy between latent heat flux (*LE),* the energy equivalent of evapotranspiration (*ET*)*,* and sensible heat flux (*H*) --where higher Bowen ratios (*H/LE*) represent increasing temperatures and lower humidity and where changes in *H* have been identified as the dominant contributor to variations in global-mean precipitation patterns (Biscaro et al., 2021; Langenbrunner et al., 2019; Myhre et al., 2018) (linking 1 and 2). Up to now, local scale observations that integrate ecosystem water and energy fluxes with vegetation dynamics in tropical forest ecosystems are scarce or do not cover multiple climatic anomalies. Here, we present for the first time an analysis of long-term tropical forest micrometeorological fluxes integrated with observations of canopy (leaf area) dynamics over a period spanning two strong El Niño-Southern Oscillation (ENSO) periods associated with anomalous wet periods (La Niña 2008-2009) and drought (El Niño 2015-2016). Long-term observations through multiple ENSO events offer unprecedented opportunities to test model

feedback mechanisms proposed to underlie changes in the global water and energy cycles, and to identify thresholds for forest tipping points at local scales.

A network of eddy covariance (EC) flux towers was installed as part of the Large-Scale Biosphere Atmosphere Experiment in Amazonia (LBA), three of them located at forest sites across equatorial Amazonia, from east to west, Caxiuana (CAX), Santarém (K67) and Manaus (K34). At these sites, observations of seasonal evapotranspiration (*ET),* under conditions representative of the long term climatology, have shown to be driven by net radiation (*Rn*) (Christoffersen et al., 2014; Hasler and Avissar, 2007). This relationship indicates a strong environmental (e.g. energy availability as key driver), and although important, a less significant biological control (e.g. stomatal resistance) over water fluxes. However, these analyses did not cover anomalous precipitation events nor periods when the meteorology showed sustained departures from the average seasonal radiation, temperature or atmospheric demand (Rosolem et al., 2008). Therefore, two key questions remain unanswered: what would be the seasonal meteorological conditions and ecosystem responses associated (1) to *drought* --will water limitation result in reductions on ecosystem-scale transpiration (and consequently *ET*) via stomatal closure? and (2) to *excess water* --when solar radiation and air temperature are often reduced due to cloud cover --will lower available energy and high soil and atmospheric moisture result in lower water flux rates? These questions provide the context for investigating whether hydrological extremes could trigger that kind of threshold-crossing reductions in forest function that constitute a tipping point.

Our study site is located near the town of Santarém, Brazil, within the Tapajós National Forest, at the K67 eddy covariance tower. The site experiences a long dry season (five-months) and represents the driest quartile of equatorial evergreen tropical forest in Amazonia (Nepstad et al., 2002; Saleska et al., 2003). The eastern Amazon region and in particular the Tapajós-Xingu moist forests are thought to be highly vulnerable to climate change and deforestation (Feeley and Rehm, 2012). Moreover, past precipitation and SST records suggest the Santarém region to be the ideal location for study of ENSO impacts as the extended multivariate ENSO index (MEI.ext) is maximally negatively correlated with precipitation anomalies (Figure 1a and S9b). The site has 12+ years of observations of water and energy fluxes that include the 2015-2016

period, when the MEI.ext pointed to drought conditions similar to those experienced in 1982-1983 and 1997-1998 and correlated with extreme droughts and heat waves across the basin (Huang et al., 2016; Jiménez-Muñoz et al., 2016). By contrast, measurements during the 2008-2009 La Niña event when the wet season was wetter and incoming solar radiation was lower than the seasonal average represent the other side of drought(Chen et al., 2010; Filizola et al., 2014). Our analysis compares the seasonal 2015-2016 El Niño and the wet La Niña water and energy fluxes to measurements before and after these events (2001-2005, 2008-2011, 2015-2020), meteorological variables and partition *ET* into its components evaporation (*E*) and transpiration (*T*) as to characterize ecosystem-atmosphere exchange under the long-term climatology and under climatic anomalies.

Our work focuses on addressing four specific questions: (1) how does the partition of available energy between sensible and latent heat change under drought/wet conditions? Does *H* dominate the turbulent fluxes during El Niño periods? (2) What is the seasonal partition of *ET* components under the long-term climatology? During different climatic anomalies, which of the *ET* constituents, evaporation (*E*) or canopy transpiration (*T*), dominates the flux? (3) Does the seasonal relationship between meteorological variables and *E, T,* and *ET* change under abnormally dry or wet conditions? (4) Do different vegetation responses --leaf abscission versus lower canopy conductance-- contribute to reducing water loss? Is there a precipitation/soil moisture threshold beyond which canopy resistance assumes a more significant role in determining seasonal *T* at K67? Our analysis aims to contribute to the understanding and prediction of the consequences of wet events and/or drought on ecosystem function in tropical forests. This includes the identification of threshold-crossing tipping points, defined by abrupt non-linear changes in forest function. We aim to gain valuable insights into the processes that drive the land-atmosphere exchange, and ultimately, the implications of extreme events on the global energy and water balance.

2. Methods

Our study site is located at the Tapajós National Forest, near the confluence of the Amazon and Tapajós rivers in Brazil (2.857°S, 54.959°W) (Figure 1). The forest canopy has an average height of 40 m and is dominated by *Erisma uncinatum, Chamaecrista xinguensis and Coussarea*

albescens (22% total basal area) (Barros et al., 2019). Water table level is at 100 m depth (Nepstad et al., 2002) and soils are classified as clay Oxisols (Oliveira et al., 2005). For additional information refer to the works by Saleska et al. (2003), Rice et al. (2004), Pyle et al. (2008), and Hutyra et al. (2007)**.**

2.1. Eddy covariance and meteorological measurements

Eddy covariance (EC) instrumentation was placed in 2000 at an 64 m tall tower, since then water and energy fluxes were measured by the close path method (Foken et al., 2012; Wofsy et al., 1993). The measurement system consists of a CSAT3 anemometer and a LI-6262 infrared gas analyzer installed 58 m above the ground (~18 m above the top of the canopy). The system was calibrated (zero or no H_2O flux) every four hours using N_2 dry air gas. The H_2O span was determined using an ancillary chilled mirror hydrometer (2000-2006), establishing air moisture at saturation (night time) or via a relative humidity probe (HC2-S3-L, since 2017). The measurements included the flux of water (F_{H2O}; mmol m^{-2} s^{-1}), sensible heat (H; W m^{-2}) and the momentum (τ; kg m^{-2} s^{-2}) as proportional to the mean covariance between fluctuations of vertical velocity measured by the anemometer and the correspondent scalar -- water vapor, temperature and horizontal wind velocity, respectively (Oke, 2015). Fluxes correspond to the periods: April 2001 - January 2006, July 2008 - July 2012 and January 2015 - July 2020. Hourly turbulent fluxes were subject to quality control, by removing rainy periods, outliers due to instrument malfunction (e.g. pump failure) or when the calibration system failed (e.g. N_2 gas run-out). The F_{H2O}, and H were filtered for low turbulence periods using the friction velocity (u_*, m s^{-1}) threshold value ($u_{*threshold}$<0.22) (Restrepo-Coupe et al., 2017). During such periods turbulence is insufficient to support eddy covariance transport of fluxes, and other transport mechanisms apply, resulting in underestimated flux. We did not gap-fill fluxes or meteorological data beyond 24 continuous hours. Missing values within 3 hour periods were filled by averaging nearby valid measurements from the previous and following hours. Additionally, within 24 hour periods we used data from the same time on the previous and following day, searching up to five consecutive days.

Ancillary measurements of net radiation (Rn; W m^{-2}) were made at 62 m above the ground with a Q-7.1 Delta-T (2002-2006) and a NR-LITE2 Campbell Sci. (2008-present). Incoming and

reflected photosynthetic active radiation (PAR and PAR_{out}, respectively; μmol m^{-2} s^{-1}) was measured at the top of the tower and at 15 m above the surface (PAR_{canopy}; μmol m^{-2} s^{-1}) using LI-190SA and LI190SB-L sensors. We measured air temperature (T_{air}; °C) using an array of Omega ON-905-44032 thermistor probes inside MetOne 076B-4 aspirators, and H_2O (mmol mol^{-1}) concentrations across a vertical profile, at 62, 57, 39 (close to average canopy height), 28, 18, 10, 3 and 0.6 m above the surface via a LI-6262 infrared-gas analyzer. The atmospheric pressure (P_a; kPa) was measured with a MKS BARATRON 122BA-00100BB Pressure Transducer 100-Torr Capacitance Manometer at ground level.

2.2. Measurement and calculation of water and energy cycle components

We used the energy balance closure equation to quantify the quality and uncertainty of the measured fluxes and to better understand the partition between turbulent, soil and storage heat fluxes (see supplementary information (SI) section 1, Figure S1-S3):

$$LE + H = Rn - G - \Delta S_H - \Delta S_{LE} - E_P - \Delta S_B - A_d - E_x \quad \text{Equation 1}$$

where the latent heat flux (LE; W m^{-2}) is the energy equivalent of F_{H2O}, G is the ground heat flux, E_P is the energy used for photosynthesis, ΔS_B is the change in biomass heat storage, A_d is the advection loss, and ΔS_H and ΔS_{LE} are the change in canopy-air space latent and sensible heat stored in the air column, respectively. The E_x includes the measurement error and additional energy sinks and heat storage components (Oliphant et al., 2004; Wilson et al., 2002). All terms are in units of W m^{-2}. The G and A_d terms were not measured and were assumed to average to zero over diel cycles. A_d is often negligible, particularly at daytime as turbulence is strong. Likewise, G is typically small for dense forests (Purdy et al., 2016), however may be significant particularly during heavy rainfall (Zawilski, 2021). We calculated ΔS_H and ΔS_{LE} following McCaughey and Saxton (1988):

$$\Delta S_H = \left(\rho_a C_p \sum_{i=1}^{h} \frac{\Delta T_{air\,i}}{\Delta t} \Delta z_i\right) \quad \text{Equation 2}$$

$$\Delta S_{LE} = \left(\rho_a \lambda \sum_{i=1}^{h} \frac{\Delta a_i}{\Delta t} \Delta z_i\right) \quad \text{Equation 3}$$

where C_p is the specific heat of air at constant pressure (1.013 10^{-3} J kg^{-1} K^{-1}), i are each of the eight vertical-heights below the EC where the profile air intakes are located, $\Delta T_{air\ i}$ represents the average change in T_{air} at level i, Δt is 1-hour (s), Δz_i is the air column thickness at level i (m) and Δa_i is the change in absolute humidity at level i (originally in units of vapor pressure, kPa -- 2.17/(T_{air} + 273.15) was used as conversion factor). λ is the latent heat of vaporization (MJ kg^{-1}) and was calculated as a function of T_{air}. ρ_a is the density of air at constant pressure (kg m^{-3}) from the ideal gas law, see Brutsaert (1982). We present values of maximum ΔS_H ($\Delta S_{H\ max}$) and ΔS_{LE} ($\Delta S_{LE\ max}$) as seasonal values of storage in general balance to zero.

ΔS_B as the product of canopy-specific heat capacity (C_{veg} = 2958 J kg^{-1} K^{-1}), live wet biomass (m_{veg}; kg m^{-2}) and the change in temperature at canopy level ($\Delta T_{cpy}/\Delta t$; K s^{-1}) (measured at 39 m height). The m_{veg} was estimated to be 63 kg m^{-2} (the equivalent of 32.5 kg m^{-2} dry biomass) (Hunter et al., 2013). The E_p was calculated assuming 28 W m^{-2} energy units per 2.5 mgCO_2 m^{-2} s^{-1} of gross ecosystem productivity (*GEP;* µmolCO_2 m^{-2} s^{-1}) (Masseroni et al., 2014). The net ecosystem exchange (*NEE*; µmolCO_2 m^{-2} s^{-1}) was calculated as the sum of the CO_2 flux measured at the top of the tower (*Fc*; µmolCO_2 m^{-2} s^{-1}) and the storage flux (S_{CO2}; µmolCO_2 m^{-2} s^{-1}) and defined as negative to represent carbon-uptake by the forest. We estimated the ecosystem respiration (R_{eco}; µmolCO_2 m^{-2} s^{-1}) and calculated the gross ecosystem exchange (*GEE*; µmolCO_2 m^{-2} s^{-1}) by subtracting R_{eco} (*GEE* = -*NEE* + R_{eco}) (see Restrepo-Coupe et al. (2017) for methods).

The *Bowen* ratio was calculated as the ratio of 16-day average sensible heat to 16-day average latent heat (*Bowen* = *H/LE*). In tropical forests, the *Bowen* ratio is typically < 1, thus as *LE* is the main driver of energy transfer from the surface to the atmosphere in this particular ecosystem. We compared the observed *LE* to the equilibrium evaporation (LE_{eq}; W m^{-2}), defined as the evaporation rate of a saturated surface into saturated air:

$$LE_{eq} = \frac{\delta}{\delta + \gamma} Rn \qquad \text{Equation 4}$$

where γ is the psychrometric coefficient (kPa K^{-1}) ($\gamma = C_p\ P_a\ 10^3$ / 0.622 λ) and δ is the slope of vapor pressure curve (δ = 4098 e_{sat} / T_{air}^{-2}; kPa K^{-1}). The LE_{eq} is used on the Priestley-Taylor

coefficient (α_{PT}) that normalizes *LE* to the climatological expectation ($\alpha_{PT}=LE/LE_{eq}$) (Eichinger et al., 1996; Holtslag and Van Ulden, 1983; Priestley and Taylor, 1972; Raupach, 2001).

2.3. Evapotranspiration components and controls

To study the water cycle we calculated evapotranspiration (*ET*; mm d^{-1}) from F_{H2O}, and estimated the stomatal resistance to water vapor (r_{sV}; m^2 s mol^{-1}) and corresponding ecosystem canopy conductance (*Gs*; mol m^{-2} s^{-1}) following the flux-gradient method as described by Wehr and Saleska (2015). *Gs* represents the vegetation contributions to *ET* fluxes, quantifies plant stress, and drives models of ecosystem photosynthetic activity. The *Gs* was calculated only for observations with no rainfall in the previous 12 hours, assuming the relatively dry conditions that will be representative of periods when water exchange will be dominated by transpiration rather than direct evaporation. We compared *Gs* calculated via the flux-gradient method to that derived from the Penman-Monteith method (Gs_{PM}). Where the Gs_{PM} was calculated for all available observations, including periods dominated by transpiration or soil evaporation. See SI Section 2 and Figures S4 and S5 for *Gs* and Gs_{PM} equations and parametrization. To understand the effect of vegetation controls on water fluxes we separately estimated evaporation (*E*) and transpiration (*T*) following the partitioning approach of Li et al. (2019). (Please refer to Stoy et al. (2019) for a discussion on other partition methods and their uncertainty.) The *ET* partition model is based on the assumption, that canopy conductance is proportional to photosynthetic activity *GEP* (mol_{CO2} m^{-2} s^{-1}) and that it can be derived from a statistical regression relating observed canopy conductance (Gs_{PM}) to observed *GEP*:

$$Gs_{PM} = G_0 + G_1 \left(\frac{GEP}{VPD_{leaf}^{m}} \right) + error \qquad \text{Equation 5}$$

where G_0 (mol m^{-2} s^{-1}), G_1 (kPa mol μmol^{-1}) and *m* are fitted parameters calculated for each 16-day interval. The two terms, G_0 and G_1 are assumed to represent soil (G_{soil}) and vegetation conductance (G_{veg}), and *E* and *T* to be proportional to the respective soil and vegetation conductance components, i.e. *E* and *T* were calculated as: $T/ET = G_{veg}/Gs_{PM}$ and $E/ET = G_{soil}/Gs_{PM}$ under the conservation constraint ($ET = E + T$). The Gs_{PM} calculated for all available daytime hours and in units of mol m^{-2} s^{-1} was decomposed into soil (G_{soil}) and canopy conductance (G_{veg}), where $G_{soil} = G_0$ and $G_{veg} = G_1\ GEP/VPD_{leaf}^{m}$. The parameter *m* varies according to the optimal stomatal control model from 0.5 (Medlyn et al., 2012) to 1 (Leuning,

1995). When fitting the linear regression (Equation 5), *m* was selected as the parameter with the highest R^2 and lower root mean square error (RMSE) value across a range of possible values (m = 0.5, 0.55, 0.6 up to 1.0) (see SI section 3). If G_0 was negative, the regression was forced to a zero intercept (no *E*). The leaf level vapor pressure deficit (VPD_{leaf}) was calculated as $\gamma LE/\rho_a C_p Gs$.

2.4. Leaf area index

Leaf area index (*LAI*; $m^2\ m^{-2}$) was calculated based on a simple radiation transfer model -- reflected light (PAR_{out}) is in balance to the incoming light (*PAR*) scaled by absorbed radiation (as light travels across the canopy back and forth), following Doughty and Goulden (2008):

$$2\ PAR_{out} = PAR \exp(-k\ LAI) \qquad \text{Equation 6}$$

where k is the site-specific extinction coefficient, calculated as 0.41/cos(SZA), and SZA is the solar zenith angle (deg). Calculations were limited to measurements dominated by direct radiation (*PAR*>1400 μmol $m^{-2}\ s^{-1}$) and SZA close to zenith (*SZA*<30). We refer to the obtained *LAI* values as LAI_{fnPAR} (Figure S5). For a comparison between different *LAI* measurement methods see SI Section 4.

2.5. Ancillary datasets

We obtained precipitation and CI daily observations from the Brazilian Institute of Meteorology (INMET) meteorological station located at the near-by town of Belterra (2.63 S, 54.95 W) --with measurements three times a day 0:00, 12:00 and 18:00 hours and daily totals, respectively. We sampled monthly 0.25 degree resolution precipitation (P_{TRMM}; mm) data (1998-2019) from the Tropical Rainfall Measuring Mission (TRMM) data product (TMPA/3B43-v7) for the K67 site and the basin. P_{TRMM} was calculated using TRMM and GOES-PI satellite observations and is calibrated using a global network of gauge data (Huffman et al., 2007). For the year 2020 we sampled the Global Precipitation Measurement Mission (GPM-IMERG final run: 2000-2020) (Huffman et al., 2014). TRMM and GPM series were overlapped and GPM precipitation was scaled to match TRMM values, because GPM tended to overestimate rainfall values measured at the tower and Belterra station. Dry season was determined using a threshold value of 100 mm

month^{-1} (Sombroek, 2001). Satellite-derived measurements of rainfall allowed us to fill periods with no or unreliable observations.

We present satellite derived incoming all-sky shortwave flux ($SW_{down\ \mathrm{CERES}}$; W m^{-2}) and net radiation (Rn_{CERES} ; W m^{-2}) from the Clouds and the Earth's Radiant Energy System (CERES) where the top of the atmosphere net flux has been energy balanced (e.g. net flux constrained to the ocean heat storage) and filled (Kato et al., 2012). Monthly 1-degree resolution cell values were sampled for the tower location from the L3B EBAF-Surface (v4) global grid.

2.6. Measures of drought: Multivariate ENSO Index (MEI), precipitation anomalies, and cumulative water deficit (CWD)

For our analysis we obtained the extended Multivariate ENSO Index (MEI.ext) values for 1900-2020 (NOAA, 2020). The MEI.ext values have been normalized so the bimonthly 1950 to 1993 time series has an average of zero and a standard deviation of one and a weak to strong El Niño is associated with a MEI.ext value greater than one (Wolter & Timlin, 2011) (SI Section 5 Figure S9). We contrasted seasonal observations from the selected La Niña (2008-2009) and El Niño (2015-2016) years with other wet and drought events documented at the site (Figure S9-S10). We included comparisons to the 2002-2003 El Niño and the 2010-2011 La Niña to highlight the consistency and differences in the vegetation response to climatic anomalies, considering the characteristics of each event (Figure S11).

To identify and quantify anomalous rainfall periods we calculated monthly precipitation anomalies ($P_{TRMM\ anomaly}$) as the departure from the 1998–2020 mean ($\mu_{1998\text{-}2020}$), normalized by the standard deviation ($\sigma_{1998\text{-}2020}$) for the month (subscript n) values across the Amazon basin (Eva and Huber (eds), 2005) and at our study site (Figure S9 and S10):

$$\mathrm{P_{TRMM\ anomaly}} = \frac{P_{\mathrm{TRMM}} - \mu_{1998\text{-}2020,n}}{\sigma_{1998\text{-}2020,n}} \qquad \text{Equation 7}$$

Similar calculations were obtained for the $SW_{down\ CERES}$ ($SW_{down\ CERES\ \mathrm{anomaly}}$) using the 2003-2019 time series. We calculated cumulative water deficit (CWD) for the month m following Aragão et al. (2007), as:

$$\mathrm{CWD_m} = \mathrm{CWD_{m-1}} - \mathrm{ET'_m} + \mathrm{P_{TRMM\ m}}$$

$$\text{if } CWD_m > 0 \text{ then } CWD_m = 0 \qquad \text{Equation 8}$$

where *ET'* are the flux observations filled assuming the missing period to be equivalent to the mean monthly *ET* of all available measurements. In Equation 8, CWD_m is defined to be a number <= 0, but since "negative" deficits would imply an excess of water, we report increasing water deficits (indicating increasingly dry conditions) as positive values ($CWD_m = -CWD_m$). We compared the *CWD* and soil volumetric water content (θ; $m^3\ m^{-3}$) across a 0-10 m profile (see SI Section 6 and Figure S12) and found *CWD* predicted soil water content with a good fit (R^2=0.89, RMSE = 0.006 [unitless], p <0.01) -- high hourly and seasonal *CWD* values correspond to low θ (Figure S13 and S14).

2.7. Hydrological year, derivation of monthly time series and other statistical analysis

We defined the hydrological year as running from July to the following June in order to study the ecosystem response to the dry period (July to November) and investigate any carry-over effects into the subsequent wet season. Each hydrological year (HY) is identified as HY_{YYYY}, where YYYY represents the year in which the HY starts. For example, HY_{2008} refers to the period from July 2008 to June 2009.

Monthly and 16-day fluxes and meteorological data were obtained from an average daytime daily cycle. Thus, we do not assign more weight to certain hours when the fluxes tend to be complete and vice-versa (e.g missing flux values due to afternoon rainfall events). Daytime values were selected as above a 5 W m^{-2} top of the atmosphere radiation (TOA; W m^{-2}) and labeled as $LE_{daytime}$ in the case of *LE*, $H_{daytime}$ for *H*, and so on. We calculated TOA following Goudriaan (1986) by scaling the solar constant (1370 J $m^{-2}\ s^{-1}$) as a function of the site latitude, day of year, and local time. We excluded night-time periods from monthly energy and water fluxes values (e.g. *H, LE*), as the processes controlling surface exchange are often different during nocturnal periods (e.g. day-time transpiration *vs.* possible night-time condensation), and as the size of nighttime fluxes is relatively small compared to daytime (Wilson et al., 2002). We aggregated 12 and 23 composites each one representing the monthly and 16-day average throughout all years, respectively.

Basic multiple regression models were calculated for *LE* and *H* with *Rn*, u_*, *VPD*, T_{air}, and P_{TRMM} as independent variables. We used linear, second degree polynomial, logarithmic, rectangular hyperbola and exponential regressions when appropriate, coefficients were fitted using the least squares method. We used Type II linear regressions when we acknowledged the uncertainty of both variables and/or wanted to minimize the effect of outliers. We described the statistical significance of all models using either the coefficient of determination (R^2) or the Pearson correlation coefficient (R) and the p-value as a measure of probability (where $p<0.01$ indicates strong evidence against the null hypothesis --no correlation between variables). We calculated the 95% confidence intervals of the slope and intercept of the linear regressions when necessary. All models and calculations were implemented in Matlab 2019b.

3. Results

To understand the forest ecosystem response to drought and wet events we compared the all-time K67 seasonality of meteorological variables and fluxes to the annual cycle during the 2008-2009 La Niña and the 2015-2016 El Niño hydrological years. To study the mechanisms that drive the seasonal surface-atmosphere water and energy exchange and how they changed under extreme weather events we performed regression analysis and calculated other ecological indicators of vegetation response (e.g.: *Gs* and *Bowen* ratio).

3.1. Characterizing meteorology during the La Niña HY2008 and the El Niño HY2015 at K67

The forest received ~24 mm month^{-1} (120 mm) during the 5-month period July-November 2015 (El Niño event), 40% of the average 62 mm month^{-1} (311 mm) dry-season precipitation (1998-2020). The HY2015 wet season onset was delayed, as rainfall values as low as 15.3 mm month^{-1} extended up to the end of February 2016 (Figure 1c). The mean total annual precipitation was 1985 mm (1998-2019) compared to 945 mm measured during the 2015-2016 El Niño and the *CWD* reached a maximum of 600 mm by mid-wet season (figure not shown). By contrast, the 2008-2009 La Niña annual precipitation was 20% higher (2404 mm) than the 1998-2019 mean, with a dry-season precipitation (265 mm) not significantly different from the average (± one standard deviation).

Typically the *VPD*, T_{air}, *Rn*, and u_* reached a maximum during the dry-season and low values were typical of the wet-period. However, we observed higher than average seasonal daytime *VPD*, T_{air}, *Rn*, and u_* values during the HY2015 and in particular the October 2015-February 2016 period (mid dry to mid wet-season). By contrast, SW_{down} during the 2008-2009 La Niña event, and in particular during the wet season - was lower than the 2001-2020 mean. The reductions in available energy correlated with increasing cloudiness and sustained significant reductions in $T_{air\ daytime}$ and $VPD_{daytime}$ (Figure 1 and 2).

3.2. Long-term and mean annual cycles of water and energy fluxes.

Long-term measurements of water and energy fluxes (Figure 2a) revealed that the sensible (*H*) and latent heat flux (*LE*) reached their annual maximum during the middle of the dry-season, gradually decreasing to a minimum 2-months after the onset of the wet-season (Figure 2d and f). However, during the 2015-2016 El Niño the $LE_{daytime}$ reached an all-time minimum (78 W m^{-2}) that was significantly earlier (in late dry season) and lower than the annual average minimum (130 ± W m^{-2}) (in the early wet season), while the seasonal $H_{daytime}$ reached sustained 16-day average daytime values above 90 W m^{-2} (up to 106 W m^{-2}) by the middle of the wet-season -- compared to the maximum of 75 ± 10 W m^{-2} characteristic of the dry period (Figure 2d). Similarly, 2015-2016 maximum seasonal values of ΔS_H were higher (25 W m^{-2}) than the average (20±2 W m^{-2}) (Figure S15a). The anomalous HY2015 seasonal pattern of *H* and *LE* can be clearly seen in the Bowen ratio (describing the dominant type of heat transfer), which shows exceptionally high values October 2015-February 2016 (Figure 2e). By the end of the dry season of the 2015-2016 ENSO, the Bowen ratio was 0.6, doubled from 0.3 --the all time average. By contrast, during the HY2008 dry-season H, LE, $\Delta S_{H\ max}$ and *Rn* were either not statistically different or lower than the all time mean.

Both *H* and *LE* fluxes did follow the available energy (*Rn*). The $Rn_{daytime}$ explained ~70% of the seasonal $LE_{daytime}$ flux (2001-2020) (R^2 = 0.7, slope = 0.5) (Figure S17). The slope of the $Rn_{daytime}$ *vs.* $LE_{daytime}$ regression decreased during the ENSO 2015-2016, thus for seasonal $Rn_{daytime}$ values lower than 300 W m^{-2} the $LE_{daytime}$ remained below average (Figure 2 and S11). Other linear regression models between $LE_{daytime}$ and $T_{air\ daytime}$ and $VPD_{daytime}$ showed significant positive correlations when derived for non-ENSO observations, however, during the HY2015

these relationships were not statistically significant (low R^2 and p-values>0.01) (Figure S16). By contrast, *CWD* did show a significant negative correlation to $LE_{daytime}$ during the 2015-2016 El Niño (R^2 = 0.51, p-value<0.01) and no correlation for years representative of the long-term climatology (R^2 = 0.2) (Figure S16).

The regression between *LE* and canopy stomatal conductance (*Gs*) was linear and highly significant during the HY2015 (R^2 =0.4, p<0.01), with no correlation observed for non-ENSO observations (Figure S17). In general, *Gs* decreased as *CWD*, $T_{air\ daytime}$ and $VPD_{daytime}$ increased (R^2 = 0.1, 0.3 and 0.5 respectively, all but *CWD* p-values<0.01). The $T_{air\ daytime}$ and $VPD_{daytime}$ *vs.* *Gs* linear regressions were maintained during the El Niño and La Niña (slope and intercept ±confidence intervals), however, the intercept of *Gs vs. CWD* increased during HY2008 and decreased during HY2015 (Figure S16). Seasonal *Gs* decreased as the dry season progressed reaching a minimum of 0.3 ±0.06 mmol m^{-2} s^{-1} at the transition to the wet period when it started to gradually increase up to a maximum of ~0.52 ±0.1 mmol m^{-2} s^{-1} (Figure 3a and c). The *Gs* remained below average until mid-2019 (Figure 3b and 3c).

Comparing two El Niño drought events, HY2015 and HY2002, we observed similar precipitation and *CWD* patterns. However, lower temperatures and *VPD* during the 2002-2003 period modulated the effects of the drought on *Gs* and $LE_{daytime}$ (Figure S10 and S11). During the 2002-2003 drought *Gs* increased both in the mid-dry and mid-wet seasons, surpassing the 16-day average of all observations. Likewise, $LE_{daytime}$ and LAI_{fnPAR} was high during the 2002-2003 drought and low during the HY2015 ENSO. By contrast, the *Gs* was high during the HY2008 La Niña. The seasonal patterns of $LE_{daytime}$, $H_{daytime}$ and *Gs* characteristic of the HY2008 wet year were similar to those observed during another La Niña event in 2010-2011 (Figure S11).

3.3. Mean annual cycles of evaporation and transpiration

Partitioning of evapotranspiration (*ET*) into evaporation (*E*) and transpiration (*T*) showed *T* dominating ecosystem water fluxes (6 mm d^{-1} average daytime *T* vs 1 mm d^{-1} *E*). Although, *Gs* decreased as the dry season progressed, the greater proportional dry season increase in *VPD* -- amplified by higher *LAI* with dry season leaf flush (Wu et al., 2016) drove *T* to reach its maximum mid-dry season. We found that *T* was significantly and generally explained by linear

regressions with SW_{down} ($R^2 = 0.2$) and LAI_{fnPAR} ($R^2 = 0.1$) (Figure 4). The relationship between seasonal *T* and soil moisture (*CWD* as proxy) was more complex, with a second degree polynomial regression between *T* and *CWD* ($R^2 = 0.1$), with increasing *T* for low values of *CWD* (0 to the inflection point at 246 mm) and a gradual decline in *T* as the soil moisture was reduced (Figure 4d). Moreover, multiple regression and stepwise models showed seasonal 16-day *T* to be explained by physiology (*Gs* explicit on the derivation of *T*), phenology, meteorology, and their interactions. For example, the best Akaike Information Criterion (AIC)-selected *T* models were driven by the sum of *Gs* and the product of leaf quantity (LAI_{fnPAR}) and available energy (ET_{eq} as proxy) or the sum of *Gs* and the product of volumetric soil moisture ($\theta_{shallow}$) and available energy -- in other words, *T* was controlled by the interaction of available energy with either *LAI* or available water ($T \sim Gs + LAI*ET_{eq}$, or $T \sim Gs + \theta_{shallow}*ET_{eq}$ see Table S1).

Both ENSO events significantly changed the relationship between *T* and meteorological variables -- R^2 and the slope of the regression increased during the La Niña event compared to the non-ENSO periods -- *T* positively correlated with T_{air}, *VPD* and SW_{down} (Figure S18). By contrast, during the drought the slope of the regressions between seasonal *T* and CWD, T_{air}, *VPD,* and SW_{down} were negative (Figure 4 and S13). The LAI_{fnPAR} was the key driver of *T* during the La Niña (Figure 4e). Interestingly, hourly *T* fluxes showed a significant positive correlation to LAI_{fnPAR} even if normalized by soil moisture (Figure S19d). Direct *E* rather than *T* dominated water fluxes during the 2015-2016 drought, as seen for the relative contributions of *E* and *T* to *ET* (Figure 5 and S21, Table S2). In general, the fraction of *ET* allocated to *E* was uncorrelated to the available energy and/or soil water (Figure 4); however, during HY2015 there was a significant relationship between *E* and *CWD* and ET_{eq} ($R^2>0.2$ and p-value <0.001) (Figures 4a,b, S13a). Moreover, different from other years, we report a direct correlation between days with moderate rainfall (4-20 mm) and high *E* values during the El Niño drought (Figures S20).

4. Discussion

Ecosystem flux observations during both the unusually strong 2015-2016 El Niño event that induced drought, high temperatures, and fires across eastern equatorial Amazônia, and during the anomalously high wet-season precipitation 2008-2009 La Niña event, offered unique opportunities to study the vulnerability of tropical forests to climate change and susceptibility of

local forest to threshold-crossing tipping points. Our main findings are: (1) During the El Niño, *ET* decreased, due to a breakdown in the strong meteorological (atmospheric demand and available energy) control of transpiration fluxes, which normally prevailed consistently through both wet and dry seasons (as well as previous droughts), but which completely and uniquely reversed during the 2015 El Niño (Figure 4e, f). This breakdown is evident in both the early physiological shutdown in existing leaves (strong decline in canopy conductance per leaf area, Figure 3c), followed by substantial loss of the leaves themselves later in the year (Figure 3e). This decline was partially ameliorated by increases in evaporation (Figure 4b), but because the dominant water flux is through trees, this could not compensate for the larger decline in *T*, leading to overall *ET* decline at the November-December El Niño peak (Figure 2a and f). Consequent to the decline in *ET* (also a decline in latent energy removal) during drought, an unusually high fraction of available energy was allocated to *H,* especially evident in the abnormally high *Bowen* ratio values (Figure 2c). (2) By contrast, during La Niña we observed both *H* and *LE* decreasing relative to the mean seasonality, these reductions driven by lower energy/atmospheric (e.g. *Rn,* T_{air} and *VPD*) and vegetation (e.g. leaf quantity) demands. Here we discuss these results as an example of a local-scale forest tipping point that emerges from environmental and phenological drivers, with implications for determining forest resilience and susceptibility to climate anomalies.

4.1. What is the effect of extreme climatic events on seasonal fluxes (sensible and latent heat)?

Across the Amazon basin over the past few decades, rainfall data suggest an increase in the frequency of anomalously severe floods and droughts and the intensification of the hydrological cycle where dry season precipitation is decreasing and wet season and annual mean precipitation are increasing (Gloor et al., 2015). Here, we have shown the other side of drought, the wet ***La Niña*****,** when high precipitation and ***low available energy*** (*Rn*, u_**, VPD* and T_{air}) drove reductions in both turbulent fluxes (seasonal low *LE* and *H*) (Figure 1 and 2). Yet, we also show how an anomalously dry ***El Niño*** period, characterized by **water limitation, high T_{air} and *VPD*** changed the turbulent flux partitioning (*H>LE*) with associated feedback effects (e.g. amplifying low atmospheric humidity). These changes may have a significant influence on local and global precipitation patterns and the energy cycle (Alexander, 2016; Myhre et al., 2018; Stephens et al.,

2012). For example, a modeling study of Langenbrunner et al. (2019) found that modeled excess CO_2-induced reductions in water fluxes, transpiration, and *Gs* were responsible for the suppression of near-surface moisture and the production of a warmer, drier, and deeper boundary layer at the Amazon basin. As we anticipate that frequency and intensity of droughts will increase (IPCC, 2022; Masson-Delmotte et al., 2018) we expect anomalously high values of *H* to dominate the turbulent flux partition and *ET* and photosynthesis/transpiration to decrease as seen at our study site and across the basin in HY2015 (Botía et al., 2022; Koren et al., 2018). Moreover, these reductions in *LE* can limit cloud formation replacing their high reflectivity by the low forest albedo values significantly changing the energy balance.

4.2. Will the *ET* flux be dominated by evaporation (*E*) or by canopy transpiration (*T*) under different environmental conditions?

Vegetation relative contributions to *ET* changed during both ENSO events: *T* decreased and *E* increased during the drought and vice versa during La Niña. Our results show that the forest crossed an environmental threshold in response to the 2015-2016 El Niño, after which increased canopy resistance (along with leaf shedding) assumed a more significant role in limiting *T* and preventing the previously observed *ET*-radiation relationship, which had persisted through dry seasons and previous droughts (Hasler and Avissar, 2007; Restrepo-Coupe et al., 2017) from being realized. Considering the 2015-2016 El Niño as defining a conservative estimate of a threshold, we identify the threshold as a climatological perturbation that equals or exceeds the values of that drought (soil drought *CWD*=400 mm simultaneous with atmospheric drought *VPD*=1.78 kPa) will similarly translate into the slowing down of forest function. Previous work by Barros et al. (2019) and Tavares et al (2023) suggested that the Tapajós K67 forest should be hydraulically resilient to droughts, because it is dominated by species with greater xylem embolism resistance and higher hydraulic safety margins compared to other tropical forests. However, even if more drought-tolerant than other forests on average, Tapajós K67 also contains substantial drought-intolerant species (Powell et al., 2017) which appear to make even this forest vulnerable to drought-induced forest slowdown for droughts that reach the extremes of 2015-2016.

As mentioned, a key component of this functional slowdown was significant drought-induced reduction in *LAI* at ecosystem level, suggesting that even non-deciduous tree species experienced leaf losses due to extreme conditions. The timescale of *LAI* recovery gives a metric of the duration of drought impact, and this shows that though the drought anomaly ended in July 2016, the leaf area did not recover until a year later, around October 2017 (Figure 3). This indicates both a legacy effect of the drought on vegetation and suggests that forests can eventually recover from this level of drought once it ends. However, the above-mentioned reductions in *T* and higher in-canopy temperatures and *H*, could potentially drive further community level selection to more drought-tolerant species at K67 causing long-term changes in forest structure and makeup that are not evident in aggregate ecosystem metrics like *LAI*.

4.3. Vegetation strategies, water loss, and local tipping points during climate anomalies. Our observations suggest El Niño reduced *LAI* due to high leaf abscission (forest structure), reduced stomatal conductance (leaf physiology) and perhaps changes in leaf structure as in Medelyn et al. (2002), wherein leaf structure modifications can be carried on into the next year (leaf life span) (2-years after the end of the drought, Figure 3a) driving further reductions in *T, Gs,* and *ET* months after precipitation resumes. Moreover, high leaf abscission and low *LAI* translated into higher *E* fluxes. Similarly, during La Niña we observed lower leaf quantity values, a significant regression between *LAI* and *T,* and no relationship between *T* and *Gs*. Abnormally wet periods could bring similar forest structure changes (e.g. due to increase windthrow and lightning events), however, at Tapajós different mechanisms seem to govern the water fluxes; our observations showed how *T* is strongly related to available energy and the unfulfilled promise of photosynthetic activity. Ultimately, reductions in leaf quantity and changes in forest temperature and moisture reported during both climatic extremes may cascade to changes in forest primary productivity, plant reproduction, and related patterns of herbivory and species survival.

The comparison of two La Niña events revealed that the wet years of 2010-2011 and 2008-2009 resulted in higher *Gs*. However, only HY2008 showed lower water and energy fluxes, the differences primarily driven by declines in incoming radiation between years. The vegetation responses associated with lower SW_{down} and *Rn* may not be observed across the Amazon basin,

since water availability rather than light environment plays a more significant role in vegetation-atmosphere exchange at the southern forests (Guan et al., 2015). At K67, the seasonal changes in water and energy flux associated with wet conditions were short-lived and, in some cases, not significantly different from the long-term average. In contrast, the comparison between the two El Niño periods of 2002-2003 and 2015-2016, showed divergent patterns in vegetation strategies to limit water loss between the two droughts and in the case of HY2015, persistent changes (e.g. *Gs* remained low for three years after rainfall resumed) with significant consequences for the forest-atmosphere exchange.

Across the basin and at the site, green-up and increased net primary productivity have been found to be correlated with dry periods and higher incoming radiation (Bonal et al., 2008; Huete et al., 2006; Saleska et al., 2016), consistent with the observed higher *LAI* during a "normal" dry-season and the earlier more moderate El Niño (HY2002) (Myneni et al., 2007). However, during the focal El Niño (HY2015) drought period, we saw significant leaf loss, in accord with remote sensing products and models at larger scales (Janssen et al., 2021a; van Schaik et al., 2018), and with observations of high litter fall in an undisturbed nearby forest (Oliveira de Morais et al., 2021), suggests a wide ecosystem-level response. These leaf area reductions have been associated with increased warming and drying of the Amazonian climate (Janssen et al., 2021b; Rowland et al., 2018, 2013). Additionally, Smith et al. (2019) reported how the seasonal changes in the vertical distribution of *LAI* at K67 were more significant than the total change -- during the dry season lower canopy *LAI* decreased as the upper canopy *LAI* increased -- and how this seasonal trends were magnified during the 2015–2016 ENSO. Although it is not possible from our data to determine which species or functional types (deciduous, semi-deciduous or evergreen) drove *LAI* losses or the significance of mortality on the changes in leaf quantity these questions should be subject of future research.

We found that during the 2015-2016 El Niño the forest crossed a threshold associated with functional break-down, the result of water limitation. This **threshold** is not solely related to **rainfall/soil moisture**. The HY2015 El Niño period was characterized by unusually **high atmospheric demand and temperatures**, which were further amplified by an ongoing warming trend (Jiménez-Muñoz et al., 2016) Additionally, the 2015-2016 warming began in 2014,

peaking during the 2014 mid-wet season (Jiménez-Muñoz et al., 2016), that meant that Amazonian forests had been experiencing a pre-drought for more than two years. Across the basin, the northeastern region experienced the more significant increases in T_{air} and *VPD* and reductions in precipitation and soil moisture. Although the sensitivity of Amazonian forests to drought can be influenced by multiple factors--such as light environment, depth to water table (Costa et al., 2023), soil characteristics, duration of drought/dry-season (Guan et al., 2015), variations in temperature and atmospheric demand or species composition (e.g. deciduous vs. evergreen, vegetation hydraulic safety margins, and rooting depths) (Tavares et al., 2023) -- regional (Koren et al., 2018; van Schaik et al., 2018) and local (Botía et al., 2022) studies showed generalized forest signs of water limitation during the HY2015. We emphasize the need and importance of conducting comparative studies across diverse tropical forests as to generalize ecosystem responses to ENSO events and other climatic anomalies.

Does the Tapajós forest response to the HY2015 El Niño show that the forest experienced a local forest tipping point transition? Of the three defining criteria for tipping points -- changes that (1) lead to substantially different and degraded function, (2) are manifest abruptly (or are associated with crossing a threshold), and (3) are irreversible (or hard to reverse) -- the observed forest behavior clearly meets the first two: the change was substantial (reversing the functional dependence of forest *LE* on net radiation that had been sustained through wet and dry seasons and previous more modest droughts over the previous decade of measurements) and degraded forest water cycling function, and appeared abruptly with the crossing of drought intensity threshold reached by the 2015 drought. Since the change was reversed, forest leaf area and ability to transpire water was eventually restored, a year or so after the end of the drought (see Figure 2 and 3), we conclude that the forest did not fully transition through a tipping point. However, the slow and prolonged post-drought recovery suggests the forest is experiencing a "critical slowing down" -- a behavior, that in dynamical systems theory is a warning sign that the forest may be approaching an irreversible critical transition or a tipping point (Hirota et al., 2021; Scheffer et al., 2009; Yang et al., 2022). Thus we suggest that although a local tipping point transition has not yet occurred, the forest has likely reached a tipping point "onset", and that further or more frequent drought perturbations could result in sustained loss of leaf area and/or

mortality that will be difficult to reverse as the water cycle feedback delineated here pushes vegetation collapse into a sustained alternative degraded state.

In conclusion, using one of the longest records of eddy covariance fluxes in Central Amazonia, we showed how the available energy partition between sensible and latent heat changed under extreme hydrological events in evergreen tropical forest, (1) with *H* dominating the turbulent flux during drought (driven by plant water stress) and (2) with reductions in both fluxes (driven by lower T_{air}, *VPD*, turbulence, and incoming radiation and occasionally, higher cloud cover) during the wet period. We found that transpiration was the main mechanism driving water fluxes under typical climate conditions. However, El Niño HY2015 changed *ET*, *E, T* and their relative importance. During the La Niña wet phase, energy availability dominated *ET* and the relative contributions of *T* to the water flux increased even as overall *ET* decreased with available energy. By contrast, during the El Niño drought, vegetation water stress reduced *T* and consequently *LE* was reduced and *H* increased, which, in contrast to dry seasons and previous previous El Niño events, led in this strongest drought (warmer and dryer atmosphere) in the observational record to significant lower stomatal conductance and loss of leaf area (consistent with a strategy to avoid further water deficits), that was a feedback to further reductions in *T*. This threshold-crossing feedback pushed the forest to the onset of a tipping point, degraded ecosystem function, possibly risking sustained forest damage if strong hydrological perturbations, such as in HY2015, continue. These results demonstrate, in contrast to some modeled mechanisms that focus solely on the effect of soil moisture, that canopy leaf dynamics and vegetation controls can generally dominate *T* fluxes, and, at least at this site, they can be a key feedback triggering the onset of a local tipping point in forest functioning.

Acknowledgments

This research was funded by awards over the life of eddy flux measurements in the Tapajós National Forest, including from the Brazilian-led Large scale Biosphere Atmosphere experiment in Amazonia (under whose auspices we established tower flux measurements in 2001) with funding contributions over the years from National Aeronautics and Space Administration (NASA) LBA investigation CD-32, NASA ROSES (Award #NNX17AF65G), the GOAmazon

project, jointly funded by the US DOE, and the Brazilian science foundations FAPESP and FAPEAM, and awards from the U.S. National Science Foundation (NSF), including PIRE (#0730305), RAPID (Award #1622721), 'IsoTraits' (awards 1754803 and 1753973), Other Side of Drought (1950080), and Cascade "Hydronomics" (2106804). M.L. was supported in part by the Next Generation Ecosystem Experiments-Tropics, funded by the U.S. Department of Energy, Office of Science, Office of Biological and Environmental Research. The authors would like to thank our faithful collaborators: Janitoni (Louro) Lima da Costa, Dr. Mauro Brum, Dr. Marielle N. Smith, Dr. Lina Mercado, Daniel Amaral, Sky Dominguez and past and present technical personnel. We acknowledge the contribution of Dr Umberto Lombardo for providing the map of legal Amazonia. First author acknowledges the support from Professor Alfredo R. Huete at University Technology Sydney, David Garces, the City of Toronto Children and Human Services, and Dr. Debra Wunch and the Department of Physics at the University of Toronto.

Data Availability Statement

Flux data are available from the Ameriflux repository http://doi.org/10.17190/AMF/1245994 andhttps://www.dropbox.com/sh/8t64phdm7asu3sn/AAC-wV3Wp5QzHQR0l_WgH_ZCa?dl=0. Code can be downloaded from the following repository: https://github.com/nataliacou pe/k67.eddy.covariance. The time series data of aboveground LAI and litter are openly available at http://doi:10.3334/ORNLDAAC/862, http://dx.doi.org/10.3334/ORNLDAAC/1196 and https://doi.org/10.1111/nph.15726. Raw and other ancillary datasets are available upon reasonable request from the authors.

References

Alexander, L.V., 2016. Global observed long-term changes in temperature and precipitation extremes: A review of progress and limitations in IPCC assessments and beyond. Weather Clim. Extrem., Observed and Projected (Longer-term) Changes in Weather and Climate Extremes 11, 4–16. https://doi.org/10.1016/j.wace.2015.10.007

Amigo, I., 2020. When will the Amazon hit a tipping point? Nature 578, 505–507. https://doi.org/10.1038/d41586-020-00508-4

Aragão, L.E.O.C., Malhi, Y., Roman-Cuesta, R.M., Saatchi, S., Anderson, L.O., Shimabukuro, Y.E., 2007. Spatial patterns and fire response of recent Amazonian droughts. Geophys. Res. Lett. 34, 5 PP. https://doi.org/200710.1029/2006GL028946

Barichivich, J., Gloor, E., Peylin, P., Brienen, R.J.W., Schöngart, J., Espinoza, J.C., Pattnayak, K.C., 2018. Recent intensification of Amazon flooding extremes driven by strengthened Walker circulation. Sci. Adv. 4, eaat8785. https://doi.org/10.1126/sciadv.aat8785

Barros, F. de V., Bittencourt, P.R.L., Brum, M., Restrepo-Coupe, N., Pereira, L., Teodoro, G.S., Saleska, S.R., Borma, L.S., Christoffersen, B.O., Penha, D., Alves, L.F., Lima, A.J.N., Carneiro, V.M.C., Gentine, P., Lee, J.-E., Aragão, L.E.O.C., Ivanov, V., Leal, L.S.M., Araujo, A.C., Oliveira, R.S., 2019. Hydraulic traits explain differential responses of Amazonian forests to the 2015 El Niño-induced drought. New Phytol. 223, 1253–1266. https://doi.org/10.1111/nph.15909

Biscaro, T.S., Machado, L.A.T., Giangrande, S.E., Jensen, M.P., 2021. What drives daily precipitation over the central Amazon? Differences observed between wet and dry seasons. Atmospheric Chem. Phys. 21, 6735–6754. https://doi.org/10.5194/acp-21-6735-2021

Bonal, D., Bosc, A., Ponton, S., Goret, J.-Y., Burban, B., Gross, P., Bonnefond, J.-M., Elbers, J., Longdoz, B., Epron, D., Guehl, J.-M., Granier, A., 2008. Impact of severe dry season on net ecosystem exchange in the Neotropical rainforest of French Guiana. Glob. Change Biol. 14, 1917–1933. https://doi.org/10.1111/j.1365-2486.2008.01610.x

Botía, S., Komiya, S., Marshall, J., Koch, T., Gałkowski, M., Lavric, J., Gomes-Alves, E., Walter, D., Fisch, G., Pinho, D.M., Nelson, B.W., Martins, G., Luijkx, I.T., Koren, G., Florentie, L., Carioca de Araújo, A., Sá, M., Andreae, M.O., Heimann, M., Peters, W., Gerbig, C., 2022. The CO2 record at the Amazon Tall Tower Observatory: A new opportunity to study processes on seasonal and inter-annual scales. Glob. Change Biol. 28, 588–611. https://doi.org/10.1111/gcb.15905

Brando, P.M., Soares-Filho, B., Rodrigues, L., Assunção, A., Morton, D., Tuchschneider, D., Fernandes, E.C.M., Macedo, M.N., Oliveira, U., Coe, M.T., 2020. The gathering firestorm in southern Amazonia. Sci. Adv. 6, eaay1632. https://doi.org/10.1126/sciadv.aay1632

Brutsaert, W., 1982. Evaporation Into the Atmosphere: Theory, History and Applications, Environmental Fluid Mechanics.

Chen, J.L., Wilson, C.R., Tapley, B.D., 2010. The 2009 exceptional Amazon flood and interannual terrestrial water storage change observed by GRACE. Water Resour. Res. 46. https://doi.org/10.1029/2010WR009383

Cooper, G.S., Willcock, S., Dearing, J.A., 2020. Regime shifts occur disproportionately faster in larger ecosystems. Nat. Commun. 11, 1175. https://doi.org/10.1038/s41467-020-15029-x

Costa, F.R.C., Schietti, J., Stark, S.C., Smith, M.N., 2023. The other side of tropical forest drought: do shallow water table regions of Amazonia act as large-scale hydrological refugia from drought? New Phytol. 237, 714–733. https://doi.org/10.1111/nph.17914

Cox, P.M., Harris, P.P., Huntingford, C., Betts, R.A., Collins, M., Jones, C.D., Jupp, T.E., Marengo, J.A., Nobre, C.A., 2008. Increasing risk of Amazonian drought due to decreasing aerosol pollution. Nature 453, 212–215. https://doi.org/10.1038/nature06960

Doughty, C.E., Goulden, M.L., 2008. Seasonal patterns of tropical forest leaf area index and CO2 exchange. J. Geophys. Res. 113, 1–12. https://doi.org/200810.1029/2007JG000590

Eichinger, W.E., Parlange, M.B., Stricker, H., 1996. On the Concept of Equilibrium Evaporation and the Value of the Priestley-Taylor Coefficient. Water Resour. Res. 32, 161–164. https://doi.org/10.1029/95WR02920

Eltahir, E. a. B., Bras, R.L., 1994. Precipitation recycling in the Amazon basin. Q. J. R. Meteorol. Soc. 120, 861–880. https://doi.org/10.1002/qj.49712051806

Esquivel-Muelbert, A., Baker, T.R., Dexter, K.G., Lewis, S.L., Brienen, R.J.W., Feldpausch, T.R., Lloyd, J., Monteagudo-Mendoza, A., Arroyo, L., Álvarez-Dávila, E., Higuchi, N.,

Marimon, B.S., Marimon-Junior, B.H., Silveira, M., Vilanova, E., Gloor, E., Malhi, Y., Chave, J., Barlow, J., Bonal, D., Davila Cardozo, N., Erwin, T., Fauset, S., Hérault, B., Laurance, S., Poorter, L., Qie, L., Stahl, C., Sullivan, M.J.P., ter Steege, H., Vos, V.A., Zuidema, P.A., Almeida, E., Almeida de Oliveira, E., Andrade, A., Vieira, S.A., Aragão, L., Araujo-Murakami, A., Arets, E., Aymard C, G.A., Baraloto, C., Camargo, P.B., Barroso, J.G., Bongers, F., Boot, R., Camargo, J.L., Castro, W., Chama Moscoso, V., Comiskey, J., Cornejo Valverde, F., Lola da Costa, A.C., del Aguila Pasquel, J., Di Fiore, A., Fernanda Duque, L., Elias, F., Engel, J., Flores Llampazo, G., Galbraith, D., Herrera Fernández, R., Honorio Coronado, E., Hubau, W., Jimenez-Rojas, E., Lima, A.J.N., Umetsu, R.K., Laurance, W., Lopez-Gonzalez, G., Lovejoy, T., Aurelio Melo Cruz, O., Morandi, P.S., Neill, D., Núñez Vargas, P., Pallqui Camacho, N.C., Parada Gutierrez, A., Pardo, G., Peacock, J., Peña-Claros, M., Peñuela-Mora, M.C., Petronelli, P., Pickavance, G.C., Pitman, N., Prieto, A., Quesada, C., Ramírez-Angulo, H., Réjou-Méchain, M., Restrepo Correa, Z., Roopsind, A., Rudas, A., Salomão, R., Silva, N., Silva Espejo, J., Singh, J., Stropp, J., Terborgh, J., Thomas, R., Toledo, M., Torres-Lezama, A., Valenzuela Gamarra, L., van de Meer, P.J., van der Heijden, G., van der Hout, P., Vasquez Martinez, R., Vela, C., Vieira, I.C.G., Phillips, O.L., 2019. Compositional response of Amazon forests to climate change. Glob. Change Biol. 25, 39–56. https://doi.org/10.1111/gcb.14413

Eva, H.D., Huber (eds), O., 2005. A Proposal for Defining the Geographical Boundaries of Amazonia: Synthesis of the results from an Expert Consultation Workshop organized by the European Commission in collaboration with the Amazon Cooperation Treaty Organization - JRC Ispra, 7-8 June 2005.

Feeley, K.J., Rehm, E.M., 2012. Amazon's vulnerability to climate change heightened by deforestation and man-made dispersal barriers. Glob. Change Biol. 18, 3606–3614. https://doi.org/10.1111/gcb.12012

Filizola, N., Latrubesse, E.M., Fraizy, P., Souza, R., Guimarães, V., Guyot, J.-L., 2014. Was the 2009 flood the most hazardous or the largest ever recorded in the Amazon? Geomorphology, Morphological characterisation and fluvial processes of large rivers at different time scales 215, 99–105. https://doi.org/10.1016/j.geomorph.2013.05.028

Foken, T., Aubinet, M., Leuning, R., 2012. The Eddy Covariance Method, in: Aubinet, M., Vesala, T., Papale, D. (Eds.), Eddy Covariance, Springer Atmospheric Sciences. Springer Netherlands, pp. 1–19. https://doi.org/10.1007/978-94-007-2351-1_1

Gatti, L.V., Basso, L.S., Miller, J.B., Gloor, M., Gatti Domingues, L., Cassol, H.L.G., Tejada, G., Aragão, L.E.O.C., Nobre, C., Peters, W., Marani, L., Arai, E., Sanches, A.H., Corrêa, S.M., Anderson, L., Von Randow, C., Correia, C.S.C., Crispim, S.P., Neves, R.A.L., 2021. Amazonia as a carbon source linked to deforestation and climate change. Nature 595, 388–393. https://doi.org/10.1038/s41586-021-03629-6

Gloor, M., Barichivich, J., Ziv, G., Brienen, R., Schöngart, J., Peylin, P., Cintra, B.B.L., Feldpausch, T., Phillips, O., Baker, J., 2015. Recent Amazon climate as background for possible ongoing and future changes of Amazon humid forests. Glob. Biogeochem. Cycles 29, 1384–1399. https://doi.org/10.1002/2014GB005080

Gloor, M., Brienen, R.J.W., Galbraith, D., Feldpausch, T.R., Schöngart, J., Guyot, J.-L., Espinoza, J.C., Lloyd, J., Phillips, O.L., 2013. Intensification of the Amazon hydrological cycle over the last two decades. Geophys. Res. Lett. 40, 1729–1733. https://doi.org/10.1002/grl.50377

Goudriaan, J., 1986. A simple and fast numerical method for the computation of daily totals of crop photosynthesis. Agric. For. Meteorol. 38, 249–254. https://doi.org/doi: DOI: 10.1016/0168-1923(86)90063-8

Guan, K., Pan, M., Li, H., Wolf, A., Wu, J., Medvigy, D., Caylor, K.K., Sheffield, J., Wood, E.F., Malhi, Y., Liang, M., Kimball, J.S., Saleska, S.R., Berry, J., Joiner, J., Lyapustin, A.I., 2015. Photosynthetic seasonality of global tropical forests constrained by hydroclimate. Nat. Geosci. 8, 284–289. https://doi.org/10.1038/ngeo2382

Hasler, N., Avissar, R., 2007. What Controls Evapotranspiration in the Amazon Basin? J. Hydrometeorol. 8, 380–395.

Hirota, M., Flores, B.M., Betts, R., Borma, L.S., Esquivel-Muelbert, A., Jakovac, C., Lapola, D.M., Montoya, E., Oliveira, R.S., Sakschewski, B., 2021. Chapter 24: Resilience of the Amazon forest to global changes: Assessing the risk of tipping points, in: Nobre, C., Encalada, A., Anderson, E., Roca Alcazar, F.H., Bustamante, M., Mena, C., Peña-Claros, M., Poveda, G., Rodriguez, J.P., Saleska, S., Trumbore, S.E., Val, A., Villa Nova, L., Abramovay, R., Alencar, A., Rodriguez Alzza, A.C., Armenteras, D., Artaxo, P., Athayde, S., Barretto Filho, H.T., Barlow, J., Berenguer, E., Bortolotto, F., Costa, F.D.A., Costa, M.H., Cuvi, N., Fearnside, P., Ferreira, J., Flores, B.M., Frieri, S., Gatti, L.V., Guayasamin, J.M., Hecht, S., Hirota, M., Hoorn, C., Josse, C., Lapola, D.M., Larrea, C., Larrea-Alcazar, D.M., Lehm Ardaya, Z., Malhi, Y., Marengo, J.A., Melack, J., Moraes R., M., Moutinho, P., Murmis, M.R., Neves, E.G., Paez, B., Painter, L., Ramos, A., Rosero-Peña, M.C., Schmink, M., Sist, P., Ter Steege, H., Val, P., Van Der Voort, H., Varese, M., Zapata-Ríos, G. (Eds.), Amazon Assessment Report 2021. UN Sustainable Development Solutions Network (SDSN). https://doi.org/10.55161/QPYS9758

Holtslag, A. a. M., Van Ulden, A.P., 1983. A Simple Scheme for Daytime Estimates of the Surface Fluxes from Routine Weather Data. J. Clim. Appl. Meteorol. 22, 517–529. https://doi.org/10.1175/1520-0450(1983)022<0517:ASSFDE>2.0.CO;2

Huang, B., L'Heureux, M., Hu, Z.-Z., Zhang, H.-M., 2016. Ranking the strongest ENSO events while incorporating SST uncertainty. Geophys. Res. Lett. 43, 2016GL070888. https://doi.org/10.1002/2016GL070888

Huete, A.R., Didan, K., Shimabukuro, Y.E., Ratana, P., Saleska, S.R., Hutyra, L.R., Yang, W., Nemani, R.R., Myneni, R., 2006. Amazon rainforests green-up with sunlight in dry season. Geophys. Res. Lett. 33, L06405. https://doi.org/200610.1029/2005GL025583

Huffman, G., Bolvin, D., Braithwaite, D., Hsu, K., Joyce, R., Xie, P., 2014. Integrated Multi-satellitE Retrievals for GPM (IMERG), version 6.0. NASA's Precipitation Processing Center [WWW Document]. URL ftp://arthurhou.pps.eosdis.nasa.gov/gpmdata/ (accessed 7.31.20).

Huffman, G.J., Bolvin, D.T., Nelkin, E.J., Wolff, D.B., Adler, R.F., Gu, G., Hong, Y., Bowman, K.P., Stocker, E.F., 2007. The TRMM Multisatellite Precipitation Analysis (TMPA): Quasi-Global, Multiyear, Combined-Sensor Precipitation Estimates at Fine Scales. J. Hydrometeorol. 8, 38–55. https://doi.org/10.1175/JHM560.1

Hunter, M.O., Keller, M., Vitoria, D., Morton, D.C., 2013. Tree height and tropical forest biomass estimation. Biogeosciences 108385-8399. https://doi.org/10.5194/bg-10-8385-2013

Hutyra, L.R., Munger, J.W., Saleska, S.R., Gottlieb, E., Daube, B.C., Dunn, A.L., Amaral, D.F., de Camargo, P.B., Wofsy, S.C., 2007. Seasonal controls on the exchange of carbon and water in an Amazonian rain forest. J. Geophys. Res. Biogeosciences 112, 1–16.

https://doi.org/10.1029/2006JG000365
IPCC, 2022. Climate Change 2022: Impacts, Adaptation, and Vulnerability., Contribution of Working Group II to the Sixth Assessment Report of the Intergovernmental Panel on Climate Change [H.-O. Pörtner, D.C. Roberts, M. Tignor, E.S. Poloczanska, K. Mintenbeck, A. Alegría, M. Craig, S. Langsdorf, S. Löschke, V. Möller, A. Okem, B. Rama (eds.)].
Janssen, T., van der Velde, Y., Hofhansl, F., Luyssaert, S., Naudts, K., Driessen, B., Fleischer, K., Dolman, H., 2021a. Drought effects on leaf fall, leaf flushing and stem growth in the Amazon forest: reconciling remote sensing data and field observations. Biogeosciences 18, 4445–4472. https://doi.org/10.5194/bg-18-4445-2021
Janssen, T., van der Velde, Y., Hofhansl, F., Luyssaert, S., Naudts, K., Driessen, B., Fleischer, K., Dolman, H., 2021b. Drought effects on leaf fall, leaf flushing and stem growth in Neotropical forest; reconciling remote sensing data and field observations. Biogeosciences Discuss. 1–41. https://doi.org/10.5194/bg-2021-30
Jiménez-Muñoz, J.C., Mattar, C., Barichivich, J., Santamaría-Artigas, A., Takahashi, K., Malhi, Y., Sobrino, J.A., Schrier, G. van der, 2016. Record-breaking warming and extreme drought in the Amazon rainforest during the course of El Niño 2015–2016. Sci. Rep. 6, 33130. https://doi.org/10.1038/srep33130
Kato, S., Loeb, N.G., Rose, F.G., Doelling, D.R., Rutan, D.A., Caldwell, T.E., Yu, L., Weller, R.A., 2012. Surface Irradiances Consistent with CERES-Derived Top-of-Atmosphere Shortwave and Longwave Irradiances. J. Clim. 26, 2719–2740. https://doi.org/10.1175/JCLI-D-12-00436.1
Koren, G., van Schaik, E., Araújo, A.C., Boersma, K.F., Gärtner, A., Killaars, L., Kooreman, M.L., Kruijt, B., van der Laan-Luijkx, I.T., von Randow, C., Smith, N.E., Peters, W., 2018. Widespread reduction in sun-induced fluorescence from the Amazon during the 2015/2016 El Niño. Philos. Trans. R. Soc. B Biol. Sci. 373, 20170408. https://doi.org/10.1098/rstb.2017.0408
Langenbrunner, B., Pritchard, M.S., Kooperman, G.J., Randerson, J.T., 2019. Why Does Amazon Precipitation Decrease When Tropical Forests Respond to Increasing CO2? Earths Future 7, 450–468. https://doi.org/10.1029/2018EF001026
Leuning, R., 1995. A critical appraisal of a combined stomatal-photosynthesis model for C3 plants. Plant Cell Environ. 18, 339–355. https://doi.org/10.1111/j.1365-3040.1995.tb00370.x
Li, X., Gentine, P., Lin, C., Zhou, S., Sun, Z., Zheng, Y., Liu, J., Zheng, C., 2019. Simple and objective method to partition evapotranspiration into transpiration and evaporation at eddy-covariance sites. Agric. For. Meteorol.
Lovejoy, T.E., Nobre, C., 2018. Amazon Tipping Point. Sci. Adv. https://doi.org/10.1126/sciadv.aat2340
Makarieva, A.M., Nefiodov, A.V., Nobre, A.D., Baudena, M., Bardi, U., Sheil, D., Saleska, S.R., Molina, R.D., Rammig, A., 2023. The role of ecosystem transpiration in creating alternate moisture regimes by influencing atmospheric moisture convergence. Glob. Change Biol. 29, 2536–2556. https://doi.org/10.1111/gcb.16644
Masseroni, D., Corbari, C., Mancini, M., 2014. Limitations and improvements of the energy balance closure with reference to experimental data measured over a maize field. Atmósfera 27, 335–352. https://doi.org/10.20937/ATM.2014.27.04.01
Masson-Delmotte, V., Zhai, P., Pörtner, H.O., Roberts, D., Skea, J., P.R.Shukla, Pirani, A.,

Moufouma-Okia, W., C.Péan, Pidcock, R., Connors, S., Matthews, J.B.R., Chen, Y., Zhou, X., Gomis, M.I., Lonnoy, E., Maycock, T., Tignor, M., (eds.), T.W., 2018. IPCC, 2018: Global warming of 1.5°C.
AnIPCC Special Report on the impacts of global warming of 1.5°C above pre-industrial levels and related global greenhouse gas emission pathways, in the context of strengthening the global response to the threat of climate change, sustainable development, and efforts to eradicate poverty.

Medlyn, B.E., Dreyer, E., Ellsworth, D., Forstreuter, M., Harley, P.C., Kirschbaum, M.U.F., Roux, X.L., Montpied, P., Strassemeyer, J., Walcroft, A., Wang, K., Loustau, D., 2002. Temperature response of parameters of a biochemically based model of photosynthesis. II. A review of experimental data. Plant Cell Environ. 25, 1167–1179. https://doi.org/10.1046/j.1365-3040.2002.00891.x

Medlyn, B.E., Duursma, R.A., Eamus, D., Ellsworth, D.S., Prentice, I.C., Barton, C.V.M., Crous, K.Y., Angelis, P. de, Freeman, M., Wingate, L., 2012. Reconciling the optimal and empirical approaches to modelling stomatal conductance. Glob. Change Biol. 18, 3476–3476. https://doi.org/10.1111/j.1365-2486.2012.02790.x

Myhre, G., Samset, B.H., Hodnebrog, Ø., Andrews, T., Boucher, O., Faluvegi, G., Fläschner, D., Forster, P.M., Kasoar, M., Kharin, V., Kirkevåg, A., Lamarque, J.-F., Olivié, D., Richardson, T.B., Shawki, D., Shindell, D., Shine, K.P., Stjern, C.W., Takemura, T., Voulgarakis, A., 2018. Sensible heat has significantly affected the global hydrological cycle over the historical period. Nat. Commun. 9, 1922. https://doi.org/10.1038/s41467-018-04307-4

Myneni, R.B., Yang, W., Nemani, R.R., Huete, A.R., Dickinson, R.E., Knyazikhin, Y., Didan, K., Fu, R., Negrón Juárez, R.I., Saatchi, S.S., Hashimoto, H., Ichii, K., Shabanov, N.V., Tan, B., Ratana, P., Privette, J.L., Morisette, J.T., Vermote, E.F., Roy, D.P., Wolfe, R.E., Friedl, M.A., Running, S.W., Votava, P., El-Saleous, N., Devadiga, S., Su, Y., Salomonson, V.V., 2007. Large seasonal swings in leaf area of Amazon rainforests. Proc. Natl. Acad. Sci. 104, 4820–4823. https://doi.org/10.1073/pnas.0611338104

Nepstad, D.C., Moutinho, P., Dias-Filho, M.B., Davidson, E., Cardinot, G., Markewitz, D., Figueiredo, R., Vianna, N., Chambers, J., Ray, D., Guerreiros, J.B., Lefebvre, P., Sternberg, L., Moreira, M., Barros, L., Ishida, F.Y., Tohlver, I., Belk, E., Kalif, K., Schwalbe, K., 2002. The effects of partial throughfall exclusion on canopy processes, aboveground production, and biogeochemistry of an Amazon forest. J. Geophys. Res. Atmospheres 107, LBA 53-1-LBA 53-18. https://doi.org/10.1029/2001JD000360

NOAA, E.S.R.L., 2020. MEI timeseries from Dec/Jan 1940/50 up to the present [WWW Document]. Multivar. ENSO Index MEI. URL https://www.esrl.noaa.gov/psd/enso/mei/table.html (accessed 5.31.20).

Oke, T.R., 2015. Boundary Layer Climates. Routledge.

Oliphant, A.J., Grimmond, C.S.B., Zutter, H.N., Schmid, H.P., Su, H.-B., Scott, S.L., Offerle, B., Randolph, J.C., Ehman, J., 2004. Heat storage and energy balance fluxes for a temperate deciduous forest. Agric. For. Meteorol. 126, 185–201. https://doi.org/10.1016/j.agrformet.2004.07.003

Oliveira de Morais, T.M., Berenguer, E., Barlow, J., França, F., Lennox, G.D., Malhi, Y., Chesini Rossi, L., Maria Moraes de Seixas, M., Ferreira, J., 2021. Leaf-litter production in human-modified Amazonian forests following the El Niño-mediated drought and fires of 2015–2016. For. Ecol. Manag. 496, 119441.

https://doi.org/10.1016/j.foreco.2021.119441
Oliveira, R.S., Dawson, T.E., Burgess, S.S.O., Nepstad, D.C., 2005. Hydraulic redistribution in three Amazonian trees. Oecologia 145, 354–363. https://doi.org/10.1007/s00442-005-0108-2
Oyama, M.D., Nobre, C.A., 2003. A new climate-vegetation equilibrium state for Tropical South America. Geophys. Res. Lett. 30. https://doi.org/10.1029/2003GL018600
Phillips, O.L., Aragão, L.E.O.C., Lewis, S.L., Fisher, J.B., Lloyd, J., López-González, G., Malhi, Y., Monteagudo, A., Peacock, J., Quesada, C.A., Heijden, G. van der, Almeida, S., Amaral, I., Arroyo, L., Aymard, G., Baker, T.R., Bánki, O., Blanc, L., Bonal, D., Brando, P., Chave, J., Oliveira, Á.C.A. de, Cardozo, N.D., Czimczik, C.I., Feldpausch, T.R., Freitas, M.A., Gloor, E., Higuchi, N., Jiménez, E., Lloyd, G., Meir, P., Mendoza, C., Morel, A., Neill, D.A., Nepstad, D., Patiño, S., Peñuela, M.C., Prieto, A., Ramírez, F., Schwarz, M., Silva, J., Silveira, M., Thomas, A.S., Steege, H. ter, Stropp, J., Vásquez, R., Zelazowski, P., Dávila, E.A., Andelman, S., Andrade, A., Chao, K.-J., Erwin, T., Fiore, A.D., C, E.H., Keeling, H., Killeen, T.J., Laurance, W.F., Cruz, A.P., Pitman, N.C.A., Vargas, P.N., Ramírez-Angulo, H., Rudas, A., Salamão, R., Silva, N., Terborgh, J., Torres-Lezama, A., 2009. Drought Sensitivity of the Amazon Rainforest. Science 323, 1344–1347. https://doi.org/10.1126/science.1164033
Powell, T.L., Wheeler, J.K., Oliveira, A.A.R. de, Costa, A.C.L. da, Saleska, S.R., Meir, P., Moorcroft, P.R., 2017. Differences in xylem and leaf hydraulic traits explain differences in drought tolerance among mature Amazon rainforest trees. Glob. Change Biol. 23, 4280–4293. https://doi.org/10.1111/gcb.13731
Priestley, C.H.B., Taylor, R.J., 1972. On the Assessment of Surface Heat Flux and Evaporation Using Large-Scale Parameters. Mon. Weather Rev. 100, 81–92. https://doi.org/10.1175/1520-0493(1972)100<0081:OTAOSH>2.3.CO;2
Purdy, A.J., Fisher, J.B., Goulden, M.L., Famiglietti, J.S., 2016. Ground heat flux: An analytical review of 6 models evaluated at 88 sites and globally. J. Geophys. Res. Biogeosciences 121, 3045–3059. https://doi.org/10.1002/2016JG003591
Pyle, E.H., Santoni, G.W., Nascimento, H.E.M., Hutyra, L.R., Vieira, S., Curran, D.J., Haren, J., Saleska, S.R., Chow, V.Y., Carmago, P.B., Laurance, W.F., Wofsy, S.C., 2008. Dynamics of carbon, biomass, and structure in two Amazonian forests. J. Geophys. Res.-Biogeosciences 113, G00B08, 20 PP.
Raupach, M.R., 2001. Combination theory and equilibrium evaporation. Q. J. R. Meteorol. Soc. 127, 1149–1181. https://doi.org/10.1002/qj.49712757402
Restrepo-Coupe, N., Levine, N.M., Christoffersen, B.O., Albert, L.P., Wu, J., Costa, M.H., Galbraith, D., Imbuzeiro, H., Martins, G., da Araujo, A.C., Malhi, Y.S., Zeng, X., Moorcroft, P., Saleska, S.R., 2017. Do dynamic global vegetation models capture the seasonality of carbon fluxes in the Amazon basin? A data-model intercomparison. Glob. Change Biol. 23, 191–208. https://doi.org/10.1111/gcb.13442
Rice, A.H., Pyle, E.H., Saleska, S.R., Hutyra, L.R., Palace, M., Keller, M., Camargo, P.B. de, Portilho, K., Marques, D.F., Wofsy, S.C., 2004. Carbon balance and vegetation dynamics in an old-growth Amazonian forest. Ecol. Appl. 14, S55–S71.
Rosolem, R., Shuttleworth, W.J., Gonçalves, L.G.G. de, 2008. Is the data collection period of the Large-Scale Biosphere-Atmosphere Experiment in Amazonia representative of long-term climatology? J. Geophys. Res. 113, 12 PP. https://doi.org/200810.1029/2007JG000628
Rowland, L., Costa, A.C.L. da, Oliveira, A.A.R., Almeida, S.S., Ferreira, L.V., Malhi, Y.,

Metcalfe, D.B., Mencuccini, M., Grace, J., Meir, P., 2018. Shock and stabilisation following long-term drought in tropical forest from 15 years of litterfall dynamics. J. Ecol. 106, 1673–1682. https://doi.org/10.1111/1365-2745.12931

Rowland, L., Malhi, Y., Silva-Espejo, J.E., Farfán-Amézquita, F., Halladay, K., Doughty, C.E., Meir, P., Phillips, O.L., 2013. The sensitivity of wood production to seasonal and interannual variations in climate in a lowland Amazonian rainforest. Oecologia 174, 295–306. https://doi.org/10.1007/s00442-013-2766-9

Saleska, S.R., Miller, S.D., Matross, D.M., 2003. Carbon in Amazon forests: Unexpected seasonal fluxes and disturbance-induced losses. Science 302, 1554–1557.

Saleska, S.R., Wu, J., Guan, K., Araujo, A.C., Huete, A., Nobre, A.D., Restrepo-Coupe, N., 2016. Dry-season greening of Amazon forests. Nature 531, E4–E5. https://doi.org/10.1038/nature16457

Scheffer, M., Bascompte, J., Brock, W.A., Brovkin, V., Carpenter, S.R., Dakos, V., Held, H., van Nes, E.H., Rietkerk, M., Sugihara, G., 2009. Early-warning signals for critical transitions. Nature 461, 53–59. https://doi.org/10.1038/nature08227

Smith, C., Baker, J.C.A., Spracklen, D.V., 2023. Tropical deforestation causes large reductions in observed precipitation. Nature 615, 270–275. https://doi.org/10.1038/s41586-022-05690-1

Smith, M.N., Stark, S.C., Taylor, T.C., Ferreira, M.L., Oliveira, E. de, Restrepo-Coupe, N., Chen, S., Woodcock, T., Santos, D.B. dos, Alves, L.F., Figueira, M., Camargo, P.B. de, Oliveira, R.C. de, Aragão, L.E.O.C., Falk, D.A., McMahon, S.M., Huxman, T.E., Saleska, S.R., 2019. Seasonal and drought-related changes in leaf area profiles depend on height and light environment in an Amazon forest. New Phytol. 222, 1284–1297. https://doi.org/10.1111/nph.15726

Sombroek, W., 2001. Spatial and temporal patterns of Amazon rainfall. Consequences for the planning of agricultural occupation and the protection of primary forests. Ambio 30, 388–396.

Staal, A., Koren, G., Tejada, G., Gatti, L.V., 2023. Moisture origins of the Amazon carbon source region. Environ. Res. Lett. 18, 044027. https://doi.org/10.1088/1748-9326/acc676

Stephens, G.L., Li, J., Wild, M., Clayson, C.A., Loeb, N., Kato, S., L'Ecuyer, T., Stackhouse, P.W., Lebsock, M., Andrews, T., 2012. An update on Earth's energy balance in light of the latest global observations. Nat. Geosci. 5, 691–696. https://doi.org/10.1038/ngeo1580

Stoy, P.C., El-Madany, T.S., Fisher, J.B., Gentine, P., Gerken, T., Good, S.P., Klosterhalfen, A., Liu, S., Miralles, D.G., Perez-Priego, O., Rigden, A.J., Skaggs, T.H., Wohlfahrt, G., Anderson, R.G., Coenders-Gerrits, A.M.J., Jung, M., Maes, W.H., Mammarella, I., Mauder, M., Migliavacca, M., Nelson, J.A., Poyatos, R., Reichstein, M., Scott, R.L., Wolf, S., 2019. Reviews and syntheses: Turning the challenges of partitioning ecosystem evaporation and transpiration into opportunities. Biogeosciences 16, 3747–3775. https://doi.org/10.5194/bg-16-3747-2019

Tavares, J.V., Oliveira, R.S., Mencuccini, M., Signori-Müller, C., Pereira, L., Diniz, F.C., Gilpin, M., Marca Zevallos, M.J., Salas Yupayccana, C.A., Acosta, M., Pérez Mullisaca, F.M., Barros, F. de V., Bittencourt, P., Jancoski, H., Scalon, M.C., Marimon, B.S., Oliveras Menor, I., Marimon, B.H., Fancourt, M., Chambers-Ostler, A., Esquivel-Muelbert, A., Rowland, L., Meir, P., Lola da Costa, A.C., Nina, A., Sanchez, J.M.B., Tintaya, J.S., Chino, R.S.C., Baca, J., Fernandes, L., Cumapa, E.R.M., Santos, J.A.R., Teixeira, R., Tello, L., Ugarteche, M.T.M., Cuellar, G.A., Martinez, F., Araujo-Murakami, A.,

Almeida, E., da Cruz, W.J.A., del Aguila Pasquel, J., Aragão, L., Baker, T.R., de Camargo, P.B., Brienen, R., Castro, W., Ribeiro, S.C., Coelho de Souza, F., Cosio, E.G., Davila Cardozo, N., da Costa Silva, R., Disney, M., Espejo, J.S., Feldpausch, T.R., Ferreira, L., Giacomin, L., Higuchi, N., Hirota, M., Honorio, E., Huaraca Huasco, W., Lewis, S., Flores Llampazo, G., Malhi, Y., Monteagudo Mendoza, A., Morandi, P., Chama Moscoso, V., Muscarella, R., Penha, D., Rocha, M.C., Rodrigues, G., Ruschel, A.R., Salinas, N., Schlickmann, M., Silveira, M., Talbot, J., Vásquez, R., Vedovato, L., Vieira, S.A., Phillips, O.L., Gloor, E., Galbraith, D.R., 2023. Basin-wide variation in tree hydraulic safety margins predicts the carbon balance of Amazon forests. Nature 617, 111–117. https://doi.org/10.1038/s41586-023-05971-3

Trenberth, K.E., 1999. Atmospheric Moisture Recycling: Role of Advection and Local Evaporation. J. Clim. 12, 1368–1381. https://doi.org/10.1175/1520-0442(1999)012<1368:AMRROA>2.0.CO;2

van der Ent, R.J., Savenije, H.H.G., Schaefli, B., Steele-Dunne, S.C., 2010. Origin and fate of atmospheric moisture over continents. Water Resour. Res. 46. https://doi.org/10.1029/2010WR009127

van Schaik, E., Killaars, L., Smith, N.E., Koren, G., van Beek, L.P.H., Peters, W., van der Laan-Luijkx, I.T., 2018. Changes in surface hydrology, soil moisture and gross primary production in the Amazon during the 2015/2016 El Niño. Philos. Trans. R. Soc. B Biol. Sci. 373, 20180084. https://doi.org/10.1098/rstb.2018.0084

Wehr, R., Saleska, S.R., 2015. An improved isotopic method for partitioning net ecosystem–atmosphere CO2 exchange. Agric. For. Meteorol. 214–215, 515–531. https://doi.org/10.1016/j.agrformet.2015.09.009

Wilson, K., Goldstein, A., Falge, E., Aubinet, M., Baldocchi, D., Berbigier, P., Bernhofer, C., Ceulemans, R., Dolman, H., Field, C., Grelle, A., Ibrom, A., Law, B.E., Kowalski, A., Meyers, T., Moncrieff, J., Monson, R., Oechel, W., Tenhunen, J., Valentini, R., Verma, S., 2002. Energy balance closure at FLUXNET sites. Agric. For. Meteorol., FLUXNET 2000 Synthesis 113, 223–243. https://doi.org/10.1016/S0168-1923(02)00109-0

Wofsy, S., Goulden, M., Munger, J.W., 1993. Net Exchange of CO2 in a Mid-Latitude Forest. Science 260, 1314–1317.

Wolter, K., Timlin, M.S., 2011. El Niño/Southern Oscillation behaviour since 1871 as diagnosed in an extended multivariate ENSO index (MEI.ext). Int. J. Climatol. 31, 1074–1087. https://doi.org/10.1002/joc.2336

Wu, J., Albert, L.P., Lopes, A.P., Restrepo-Coupe, N., Hayek, M., Wiedemann, K.T., Guan, K., Stark, S.C., Christoffersen, B., Prohaska, N., Tavares, J.V., Marostica, S., Kobayashi, H., Ferreira, M.L., Campos, K.S., Silva, R. da, Brando, P.M., Dye, D.G., Huxman, T.E., Huete, A.R., Nelson, B.W., Saleska, S.R., 2016. Leaf development and demography explain photosynthetic seasonality in Amazon evergreen forests. Science 351, 972–976. https://doi.org/10.1126/science.aad5068

Yang, H., Ciais, P., Wigneron, J.-P., Chave, J., Cartus, O., Chen, X., Fan, L., Green, J.K., Huang, Y., Joetzjer, E., Kay, H., Makowski, D., Maignan, F., Santoro, M., Tao, S., Liu, L., Yao, Y., 2022. Climatic and biotic factors influencing regional declines and recovery of tropical forest biomass from the 2015/16 El Niño. Proc. Natl. Acad. Sci. 119, e2101388119. https://doi.org/10.1073/pnas.2101388119

Zawilski, B.M., 2021. The Soil heat flow sensor functioning checks, imbalances' origins and forgotten energies. Geosci. Instrum. Methods Data Syst. Discuss. 1–22.

https://doi.org/10.5194/gi-2021-34

List of Figures

Figure 1. (a) Correlation coefficient (R) for the linear regression between precipitation anomalies ($P_{anomaly}$) from the Tropical Rainfall Measuring Mission (TRMM v7) and the extended Multivariate ENSO Index (MEI.ext) from January 1998 to December 2019 across the Amazon Basin *sensu-stricto* (dashed-white areas correspond to the Amazon *sensu-lato*). Location of Tapajós National Forest K67 eddy covariance tower. Santarém K67 seasonal 16-day values of (b) daytime air temperature ($T_{air\ daytime}$; °C) and (c) satellite-derived precipitation (mm month^{-1}). (d) Noon time cloudiness index ($CI_{12:00}$) measured at the nearby Brazilian Institute of Meteorology (INMET) Belterra station (2000-2020). Hydrological years July 2008-June 2009 (blue line) and July 2015–June 2016 (red line) and mean (black line) and standard deviation (dark gray area) of all available observations (2002-2006, 2008-2013 and 2015-2020). July-November gray-shaded area is the average dry season defined as rainfall < 100 mm month^{-1}.

Figure 2. Santarém K67 seasonal 16-day values of average (a) long-term time series of daytime sensible heat flux ($H_{daytime}$; W m^{-2}) and (b) latent heat flux ($LE_{daytime}$; W m^{-2}). Annual composites of (c) net radiation from the Clouds and the Earth's Radiant Energy System (CERES: 2003–2020) (Rn_{CERES}; W m^{-2}), (d) $H_{daytime}$, (e) Bowen ratio (Bowen = H/LE) and (f) $LE_{daytime}$. Hydrological years July 2008-June 2009 (blue line), July 2015–June 2016 (red line) and mean (black line) and standard deviation (dark gray area) of all available observations (2002-2006, 2008-2013 and 2015-2020). July-November gray-shaded area is the average dry season defined as rainfall < 100 mm month^{-1} using satellite-derived measures of precipitation.

Figure 3. Santarém K67 seasonal 16-day values of average (a) long-term time series of leaf area index (LAI_{fnPAR}; m^2 m^{-2}), and (b) ecosystem-level canopy stomatal conductance (Gs, mol m^{-2} s^{-1}). Annual composites of (c) Gs (mol m^{-2} s^{-1}), (d) LAI_{fnPAR}, (e) transpiration (mm d^{-1}), (f) evaporation (mm d^{-1}), and (g) daytime evapotranspiration ($ET_{daytime}$; mm d^{-1}) . Hydrological years July 2008-June 2009 (blue line), July 2015 – June 2016 (red line) and mean (black line) and standard deviation (dark gray area) of all available observations (2002-2006, 2008-2013 and 2015-2020). July-November gray-shaded area is the average dry season defined as rainfall < 100 mm month^{-1} using satellite-derived measures of precipitation.

Figure 4. Santarém K67 linear regression between average 16-day seasonal daytime values of evaporation (E; mm d^{-1}) (a) to cumulative water deficit (CWD; mm), (b) incoming shortwave radiation from the Clouds and the Earth's Radiant Energy System (CERES: 2003–2020) ($SW_{down\ CERES}$; W m^{-2}) and (c) daytime vapor pressure deficit ($VPD_{daytime}$; kPa). Transpiration (T; mm d^{-1}) to (d) CWD, (e) $SW_{down\ CERES}$, and (f) $VPD_{daytime}$. Lower panels: T vs (g) leaf area index (LAI_{fnPAR}) and (h) ecosystem level canopy stomatal conductance (Gs; mmol m^{-2} s^{-1}). Hydrological years July 2008-June 2009 (blue line and dots), July 2015–June 2016 (red line and dots) and mean (gray line and dots) of all available observations (2002-2006, 2008-2013 and 2015-2020). The 95% confidence intervals for regression coefficient estimates as gray areas.

Figure 5. Santarém K67 linear regression between seasonal 16-day average daytime components of evapotranspiration --transpiration and evaporation ($ET_{component}$; mm d^{-1}) to equilibrium evapotranspiration ($ET_{eq\&day}$; mm d^{-1}). Comparing hydrological years July 2008-June 2009 (La Niña --blue line and dots), July 2015–June 2016 (El Niño --red line and dots) and all other available measurements (2002-2006, 2009-2013 and 2016-2020 --gray line and dots). ENSO years as Type II regressions. The 95% confidence intervals for regression coefficient estimates as gray areas. Refer to Table S2 for coefficients and statistical significance.

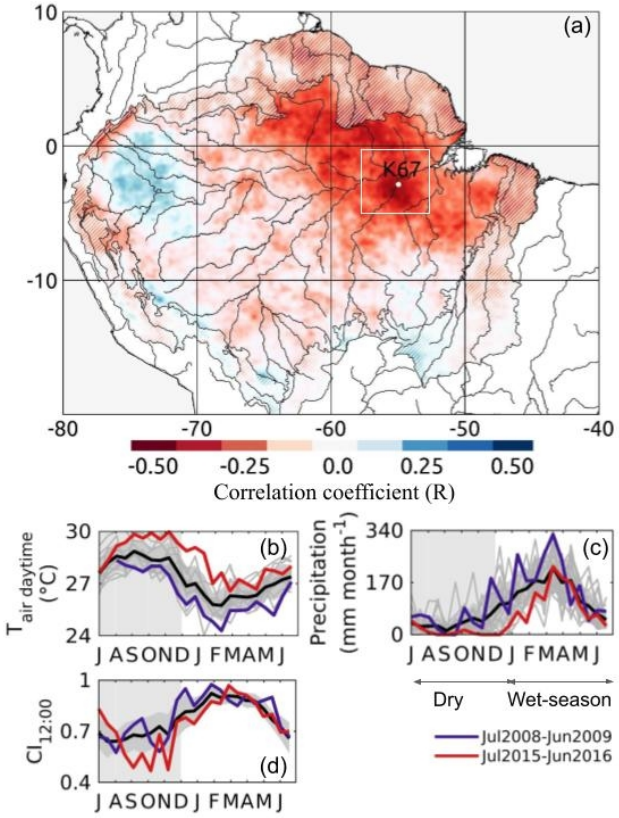

Figure 1. (a) Correlation coefficient (R) for the linear regression between precipitation anomalies ($P_{anomaly}$) from the Tropical Rainfall Measuring Mission (TRMM v7) and the extended Multivariate ENSO Index (MEI.ext) from January 1998 to December 2019 across the Amazon Basin *sensu-stricto* (dashed-white areas correspond to the Amazon *sensu-lato*). Location of Tapajós National Forest K67 eddy covariance tower. Santarém K67 seasonal 16-day values of (b) daytime air temperature ($T_{air\ daytime}$; °C) and (c) satellite-derived precipitation (mm month^{-1}). (d) Noon time cloudiness index ($CI_{12:00}$) measured at the nearby Brazilian Institute of Meteorology (INMET) Belterra station (2000-2020). Hydrological years July 2008-June 2009 (blue line) and July 2015–June 2016 (red line) and mean (black line) and standard deviation (dark gray area) of all available observations (2002-2006, 2008-2013 and 2015-2020). July-November gray-shaded area is the average dry season defined as rainfall < 100 mm month^{-1}.

287x372mm (72 x 72 DPI)

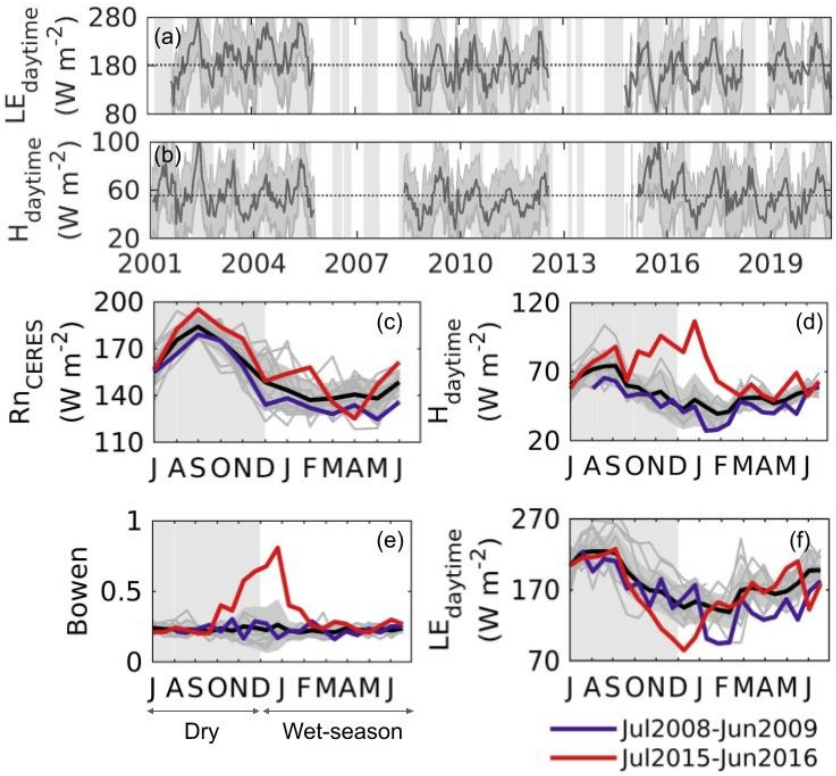

Figure 2. Santarém K67 seasonal 16-day values of average (a) long-term time series of daytime sensible heat flux ($H_{daytime}$; W m^{-2}) and (b) latent heat flux ($LE_{daytime}$; W m^{-2}). Annual composites of (c) net radiation from the Clouds and the Earth's Radiant Energy System (CERES: 2003–2020) (Rn_{CERES}; W m^{-2}), (d) $H_{daytime}$, (e) Bowen ratio (Bowen = H/LE) and (f) $LE_{daytime}$. Hydrological years July 2008-June 2009 (blue line), July 2015–June 2016 (red line) and mean (black line) and standard deviation (dark gray area) of all available observations (2002-2006, 2008-2013 and 2015-2020). July-November gray-shaded area is the average dry season defined as rainfall < 100 mm $month^{-1}$ using satellite-derived measures of precipitation.

287x372mm (72 x 72 DPI)

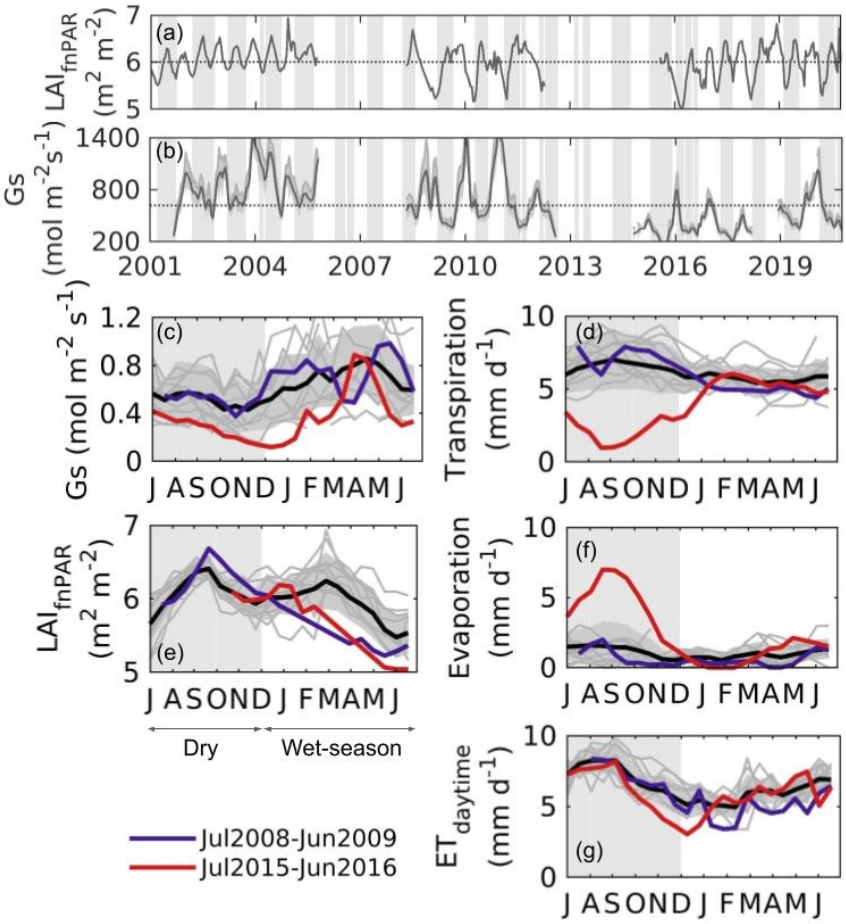

Figure 3. Santarém K67 seasonal 16-day values of average (a) long-term time series of leaf area index (LAI_{fnPAR}; m^2 m^{-2}), and (b) ecosystem-level canopy stomatal conductance (Gs, mol m^{-2} s^{-1}). Annual composites of (c) Gs, (d) LAI_{fnPAR}, (e) transpiration (mm d^{-1}), (f) evaporation (mm d^{-1}), and (g) daytime evapotranspiration ($ET_{daytime}$; mm d^{-1}) . Hydrological years July 2008-June 2009 (blue line), July 2015 – June 2016 (red line) and mean (black line) and standard deviation (dark gray area) of all available observations (2002-2006, 2008-2013 and 2015-2020). July-November gray-shaded area is the average dry season defined as rainfall < 100 mm $month^{-1}$ using satellite-derived measures of precipitation.

287x372mm (72 x 72 DPI)

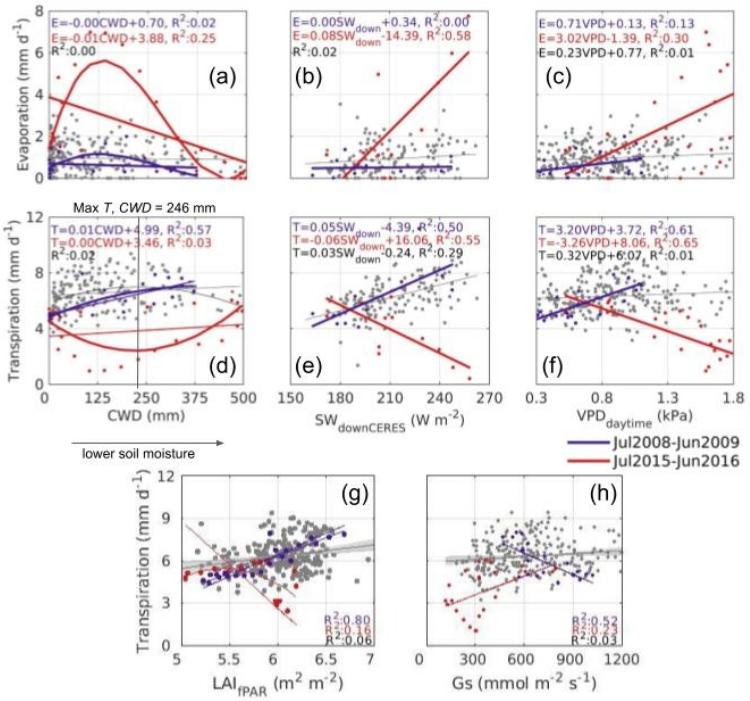

Figure 4. Santarém K67 linear regression between average 16-day seasonal daytime values of evaporation (E; mm d^{-1}) (a) to cumulative water deficit (CWD; mm), (b) incoming shortwave radiation from the Clouds and the Earth's Radiant Energy System (CERES: 2003–2020) ($SW_{down\ CERES}$; W m^{-2}) and (c) daytime vapor pressure deficit ($VPD_{daytime}$; kPa). Transpiration (T; mm d^{-1}) to (d) CWD, (e) $SW_{down\ CERES}$, and (f) $VPD_{daytime}$. Lower panels: T vs (g) leaf area index (LAI_{fnPAR}) and (h) ecosystem level canopy stomatal conductance (Gs; mmol m^{-2} s^{-1}). Hydrological years July 2008-June 2009 (blue line and dots), July 2015–June 2016 (red line and dots) and mean (gray line and dots) of all available observations (2002-2006, 2008-2013 and 2015-2020). The 95% confidence intervals for regression coefficient estimates as gray areas.

287x372mm (72 x 72 DPI)

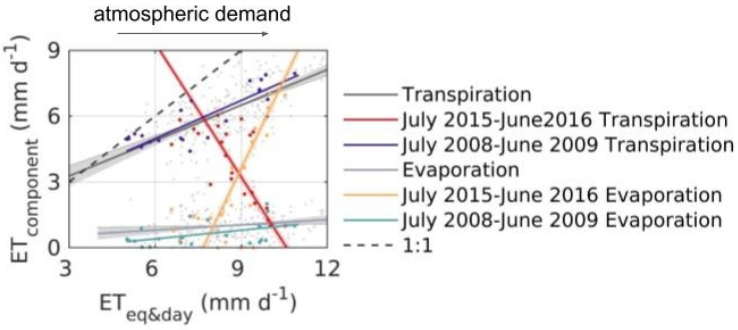

Figure 5. Santarém K67 linear regression between seasonal 16-day average daytime components of evapotranspiration --transpiration and evaporation ($ET_{component}$; mm d^{-1}) to equilibrium evapotranspiration ($ET_{eq\&day}$; mm d^{-1}). Comparing hydrological years July 2008-June 2009 (La Niña --blue line and dots), July 2015–June 2016 (El Niño --red line and dots) and all other available measurements (2002-2006, 2009-2013 and 2016-2020 --gray line and dots). ENSO years as Type II regressions. The 95% confidence intervals for regression coefficient estimates as gray areas. Refer to Table S2 for coefficients and statistical significance.

287x372mm (72 x 72 DPI)